

Chapter 2

Electrohydrodynamic and Magnetohydrodynamic Micropumps

Antonio Ramos

Departamento de Electrónica y Electromagnetismo.

Universidad de Sevilla. Avenida Reina Mercedes s/n. 41012-Sevilla,
Spain. ramos@us.es

1. Introduction

A great variety of strategies have been developed to pump fluids in microsystems. According to Laser and Santiago [1] micropumps generally fall into one of two classes: (a) displacement pumps, which exert pressure forces on the working fluid by one or more moving boundaries and (b) dynamic micropumps, which exert forces directly on the liquid, without moving parts. From the latter category, we are going to deal with micropumps that exert electric or magnetic forces on liquids, called electrohydrodynamic (EHD) or magnetohydrodynamic (MHD) micropumps, respectively. The main goal of the present work is to describe the physical principles behind the EHD and MHD micropump actuation, and what physical parameters affect the performance of these micropumps.

The transport of small volumes of liquid in microdevices is often achieved by taking advantage of passive mechanisms such as capillarity or gravity. Sometimes microfluidic applications employ macroscale pumps like syringe pumps or pressure/vacuum chambers and valves. However, many microfluidic applications would benefit from an on-chip active pump with size comparable to the small volume of fluid to be pumped, i.e. an integrated micropump. An integrated pump design that has been studied intensively over the years is the piezo-actuated micropump. In this, a membrane is displaced to create a pulsating flow that is rectified using valves. However, the moving parts make the fabrication and operation delicate. In this context, the requirement of an integrated micropump with no moving parts can be fulfilled by using EHD and MHD micropumps.

Micropumps have prominent features with length scales of the order of 0.1 mm or smaller but greater than 100 nm. Therefore, subcontinuum effects, that may be important in nanosystems, are not important here. Subcontinuum effects can also be important for the pumping of gases in microsystems; however, our study is restricted to the pumping of liquids in microsystems. Typically, fluid flows will be laminar and, in many situations, in the low Reynolds number regime.

Possible applications of micropumps [1] cover dispensing therapeutic agents into the body, cooling of microelectronic devices, dispensing liquids in miniature systems for chemical and biological analysis, micropumping of liquids in space exploration where miniaturization is highly desirable, and more.

EHD and MHD dynamic micropumps may be classified into the following:

- (a) pumps that exert electric forces in the liquid bulk: the EHD *injection* [2], *conduction* [3], and *induction* [4] *pumps*
- (b) those that exert electric forces in the diffuse double layer: the *electroosmotic* [5] and *AC induced-charge electroosmotic* [6] *pumps*
- (c) those that exert magnetic forces in the liquid bulk: the *DC* [7] and *AC* [8] *MHD* pumps

In all of them, electric current flows through the working liquid and a variety of pumping techniques is encountered depending on the conductivity of the liquids. We first deal with some basic aspects of electric conduction in liquids and some basic fluid-mechanical aspects that are common for micropumps. Secondly, for each micropump, we analyse the physical principle behind the micropump actuation. We also describe some important properties of pumps like the maximum flow rate Q_{\max} and maximum pressure Δp_{\max} that the pump can generate, the power consumption and energy efficiency, and the typical conductivity range that the pump can actuate. We discuss what kind of problems affect the performance of micropumps such as heat generation, or changes in physical properties of the working fluid and bubble generation both caused by electrochemical reactions. For each type of micropump, we address what are the possible applications. Finally, we compare the performance of the different micropumps and draw some conclusions.

1.1. Basic Features of Conduction in Liquids

Charge carriers in liquids are electrons, holes, and ions [9]. Measurements of electron and hole mobility require extremely pure dielectric liquids in order for the electron or hole to survive attachment or charge transfer,

respectively [9]. Except for liquid metals and/or ultrahigh purified noble liquids, there exist many situations where free electrons in liquids are quickly trapped by electronegative impurities or molecules of the liquid [10]. In most cases, the charge carriers in liquids will be ions in dissolution, and this is the situation we are going to consider. Under the action of the electric field, these ions can be considered to move at the terminal velocity $\mathbf{v} = \mu \mathbf{E}$ (ion inertia is negligible) [10], where μ is the mobility of the ion. A good model is to consider the ions as spheres affected by viscous friction. This provides an expression for the mobility as $\mu = q/6\pi a\eta$ (Stokes-Einstein relation), where q is the ion charge, a the hydrodynamic radius of the solvated ion, and η the dynamic viscosity of liquid. The ion charge is $q = ze$, where e is the charge of a proton and z is the valence. The mobility of ions in liquids is usually between 10^{-7} to $10^{-9} \text{ m}^2 (\text{Vs})^{-1}$. Ion motion is also affected by molecular diffusion and convection. Therefore, the electric current in the liquid bulk can be written as

$$\mathbf{j} = \sum_i q_i (n_i \mu_i \mathbf{E} - D_i \nabla n_i + n_i \mathbf{u}), \quad (1)$$

where n_i is the number density of ionic species, D_i is the diffusion coefficient of an ion, and \mathbf{u} the velocity of the fluid. The first term on the right represents ion migration in the electric field, the second describes transport of charge by diffusion, and the third the transport by convection. The diffusion and mobility coefficients of an ion are linked by Einstein's relation, $D_i/\mu_i = k_B T/q_i$, where k_B is the Boltzmann's constant and T is the absolute temperature.

In many situations common in microsystems, the diffusion current is negligible in front of the electro-migration current. If we compare diffusion and migration, $|D \nabla n|/|\mu n \mathbf{E}| \sim D/\mu E l$, where l is a typical distance. From the Einstein's relation, the ratio $D/\mu = k_B T/q \approx 0.025 \text{ V}$ at room temperature, and $E l$, the typical increment of voltage in the bulk, is usually much greater than 0.025 V . Therefore, $|D \nabla n|/|\mu n \mathbf{E}| \ll 1$. However, the diffusion current can be important close to the electrodes and walls, where double layers are formed.

For electrolytes the convective current is usually much smaller than the conduction current. In effect, the ratio between convective current and electro-migration current is of the order of

$$\frac{\rho u}{\sum_i q_i n_i \mu_i E} \sim \frac{\nabla \cdot (\varepsilon \mathbf{E}) u}{\sum_i q_i n_i \mu_i E} \sim \frac{\varepsilon u}{\sum_i q_i n_i \mu_i l}, \quad (2)$$

where $\rho = \sum_i q_i n_i$ is the charge density. For electrolytes, $\sum_i q_i n_i \mu_i$ is of the order of (or equal to, if n_i are equilibrium concentrations) the conductivity of the liquid, so the ratio is of the order of $u\epsilon/l\sigma$, which is much smaller than one [11]. For insulating dielectric liquids, the ratio between convection and ion-migration velocities, $u/\mu E$, can be greater or smaller than one.

The electric current expression (1) needs to be modified when dealing with the MHD pumping of electrolytes. In effect, from the Lorentz force on an ion $\mathbf{f} = q(\mathbf{E} + \mathbf{u} \times \mathbf{B})$, the term $\sum_i q_i n_i \mu_i \mathbf{u} \times \mathbf{B}$ should be added to the previous equation. However, it is common that the term $\mathbf{u} \times \mathbf{B}$ is negligible as compared to the electric field \mathbf{E} for electrolytes actuated with magnetic fields in microsystems (see Sect. 4).

Each ionic and neutral species satisfies a conservation equation [12]

$$\frac{\partial n_i}{\partial t} + \nabla \cdot (n_i \mu_i \mathbf{E} - D_i \nabla n_i + n_i \mathbf{u}) = r_i, \quad (3)$$

where r_i is the rate of production due to chemical reactions ($\mu_i = 0$ for neutral species).

In solutions of strong electrolytes, the majority of ions come from the dissociation of neutral salt and this is completely dissociated. In this case, there are no neutral species and no reactions in the bulk ($r_i = 0$ per each ionic species). Electrochemical reactions take place only at the electrodes.

In *unipolar injection*, there is only a single ionic species, and there is no production of charges in the bulk $r_i = 0$. The ions are produced by reactions at the electrodes.

For a weak binary $z-z$ electrolyte, there are three species: the positive ion, the negative ion, and the neutral molecule that dissociates into these ions. The ions are produced (or consumed) by reactions at the electrodes and by homogeneous chemical reactions in the bulk,

$$-r_0 = r_+ = r_- = k_d n_0 - k_r n_+ n_-, \quad (4)$$

where k_d and k_r are the dissociation and recombination rate constants and n_0 , n_+ and n_- are the concentrations of neutral, positive, and negative species, respectively.

In dielectric liquids, the charge carriers originate from dissociation of impurities in the bulk, or of the liquid itself, and/or from ions injected at the surface of the electrodes [10]. The conductivity of a dielectric liquid is

highly dependent on its dielectric constant. Ions recombine if the energy of Coulomb attraction is greater than the thermal energy $k_B T$ at the point of closest approach of the ions. The distance at which Coulomb attraction energy equals $k_B T$ is called the Bjerrun distance, $l_B = e^2 / 4\pi\epsilon k_B T$ [10]. If the solvated ions have a diameter greater than the Bjerrun distance, the ions do not recombine. For instance, $l_B = 0.7$ nm for water at room temperature, and solvated ions have a greater radius. Therefore, in water impurities tend to be dissociated. On the other hand, if the Bjerrun distance is greater than the diameter of the ions, an equilibrium is established between dissociation and recombination. Because the probability to occur dissociation is proportional to the exponential factor $\exp(-l_B/a)$, the conductivity is highly dependent on the dielectric constant ϵ_r of the liquid. In polar liquids ($\epsilon_r \gg 2$), all impurities tend to be dissociated. In contrast, in nonpolar liquids ($\epsilon_r \sim 2$) there is an equilibrium between dissociation and recombination.

To establish a DC current in a liquid, electrons should be transferred from the metal electrodes to the molecules in the liquid, and viceversa. This can happen by electron emission from surface irregularities, from electrochemical redox reactions at the surface or by other means. From the mathematical point of view, the different mechanisms are described by similar parameters [13]. A simple picture is to consider that neutral molecules can be charged at the electrodes: on the cathode $X + e^- = X^-$, on the anode $X - e^- = X^+$; and that ions can be discharged at the electrodes: on the cathode $X^+ + e^- = X$, on the anode $X^- - e^- = X$. This together with the homogeneous reactions of ion production in the bulk form a simple dissociation-injection picture of conduction in liquids [13].

In the case of AC currents, the charging of the double layer at the electrodes should be considered [14] (see also Sect. 3). A simple model is to consider the electric double layer of the electrodes as a capacitor and a resistor in parallel and both connected to a resistive liquid bulk. The current through the capacitor represents the charging of the double layer, while the current through the resistor represents the Faradaic current. In the AC case, if the voltage drop across the double layer is not high, the electrochemical reactions at the electrodes can be very much reduced. In this case, the continuity of electric current can be guaranteed with no electrochemical reactions (no faradaic current) by the charging of the double layer.

The equations that govern the electric field are those of Electro-quasi-statics. In effect, the electric field that drives the current can be considered to be irrotational if the magnetic energy density is much smaller than the electric energy density [10]. When the electric currents in the liquid are the sources of \mathbf{B} , the magnetic field intensity can be estimated from Ampère-Maxwell law

$$\nabla \times \mathbf{B} = \mu_0 \mathbf{j} + \mu_0 \varepsilon \frac{\partial \mathbf{E}}{\partial t}, \quad (5)$$

as $B \sim \max(\mu_0 j l, \mu_0 \varepsilon \omega E l)$, where ω is a typical frequency. Putting $j = \sigma E$, the ratio of energies is

$$\frac{B^2 / \mu_0}{\varepsilon E^2} \sim \max(\mu_0 \sigma^2 l^2 / \varepsilon, \mu_0 \varepsilon \omega^2 l^2). \quad (6)$$

For liquid conductivity $\sigma < 10 \text{ S m}^{-1}$ and a typical system length $l \sim 100 \mu\text{m}$, $\mu_0 \sigma^2 l^2 / \varepsilon < 0.14 / \varepsilon_r \ll 1$, where ε_r is the relative permittivity of the liquid. For frequencies smaller than 10 MHz and system length $l < 1 \text{ mm}$, $\mu_0 \varepsilon \omega^2 l^2 < 3 \times 10^{-6}$. Under these assumptions our system is in the quasi-electrostatic limit of Maxwell equations [10,15]:

$$\nabla \cdot (\varepsilon \mathbf{E}) = \rho = \sum_i q_i n_i, \quad (7)$$

$$\nabla \times \mathbf{E} = 0, \quad (8)$$

$$\nabla \cdot \mathbf{j} + \frac{\partial \rho}{\partial t} = 0. \quad (9)$$

The electric field that drives the current is also very approximately irrotational in the case of electrolytes actuated by MHD micropumps (see Sect. 4).

1.2. Mechanical Aspects of Micropumps

Liquid motion is governed by the Navier-Stokes equations for an incompressible fluid

$$\nabla \cdot \mathbf{u} = 0, \quad (10)$$

$$\rho_m \frac{\partial \mathbf{u}}{\partial t} + \rho_m (\mathbf{u} \cdot \nabla) \mathbf{u} = -\nabla p + \eta \nabla^2 \mathbf{u} + \mathbf{f}, \quad (11)$$

where \mathbf{f} represents any body force density applied to the liquid. For microsystems the Reynolds number is usually very small and the

convective term in the Navier-Stokes equations can be neglected. In effect, the Reynolds number is a measure of the ratio $|\rho_m \mathbf{u} \cdot \nabla \mathbf{u}| / |\eta \nabla^2 \mathbf{u}|$ and is given by $Re = \rho_m u l / \eta$, where l is a typical length of the system. Taking typical values in microsystems, $u \sim 10^{-3} \text{ m s}^{-1}$, $l \sim 10^{-4} \text{ m}$, it is obtained $Re \sim 0.1$ in the case of water. Therefore, viscous forces are usually dominant in front of inertial forces in microsystems [16]. Under steady-state conditions, the momentum equation is then

$$0 = -\nabla p + \eta \nabla^2 \mathbf{u} + \mathbf{f}. \quad (12)$$

To the equations of motion, we must add the boundary condition of no-slip for the velocity.

The equations relating fluid velocities to forces and pressure gradients are linear, and this linearity allows for the usual representation of microfluidic networks in terms of equivalent electrical circuits. The applied force will commonly be concentrated in a certain region of the microfluidic system, this is the micropump region, and it is equivalent to the generator of an electrical circuit. For a channel of the network outside the micropump, the volume flow rate Q is linearly related to the pressure difference Δp between the inlet and outlet of the channel. For a straight channel of circular cross section we have

$$Q = \Delta p \frac{\pi D^4}{128 \eta L}, \quad (13)$$

where D is the diameter and L length of the channel. The channel behaves as a resistor in an electrical circuit, where Q and Δp are equivalent to the current intensity and potential drop, respectively.

Two important parameters of a pump are the maximum pressure Δp_{\max} and maximum flow rate Q_{\max} that the pump can generate. The maximum flow rate is obtained when the pump actuates without an external load, that is, when the pressure difference between the inlet and outlet of the pump is zero. The maximum pressure is the pressure difference required to stop the flow that the pump generates. In many situations, the flow rate Q that a pump is able to produce against a back pressure Δp , under constant operating conditions, can be approximated by a linear relation of the form $Q = Q_{\max} (1 - \Delta p / \Delta p_{\max})$.

Power consumption and energy efficiency are important operational parameters of pumps [1]. When comparing different pumps, we would prefer the one that consumes less power for obtaining a given flow rate or

a given pressure. According to Laser and Santiago [1], the most useful definition of energy efficiency for a pump is the hydraulic power divided by the power consumption, $eff = \Delta p Q / P_{in}$. Here P_{in} is the power that goes into the pump. For instance, the total power consumption of a mechanical pump that delivers the hydraulic power $Q\Delta p$ is $Q\Delta p$ plus the friction losses of its moving parts. Therefore, the efficiency of a frictionless mechanical pump is unity. When, under constant operating conditions, there is a linear relationship between Δp and Q , the maximum energy efficiency can be calculated as

$$eff = \frac{1}{4} \frac{Q_{max} \Delta p_{max}}{P_{in}}. \quad (14)$$

We will use this expression in order to estimate the efficiencies of micropumps, even in cases where the linear relationship between Δp and Q does not hold.

2. Electric Forces in the Bulk: Injection, Conduction, and Induction EHD Pumps

When there is an electric field in a liquid, electric forces are exerted on it. The electric body force density is [17]

$$\mathbf{f}_E = \rho \mathbf{E} - \frac{1}{2} E^2 \nabla \varepsilon + \frac{1}{2} \nabla \left[E^2 \rho_m \left(\frac{\partial \varepsilon}{\partial \rho_m} \right)_T \right], \quad (15)$$

where the first term is the Coulomb force, the second term is the dielectric force, and the third is the electrostriction. The latter can be incorporated into the pressure for an incompressible fluid. A simple way of seeing that the electric field exerts forces on the fluid is to consider that the forces on the free charges and dipoles are transmitted directly to the liquid [12]. The Coulomb term represents the force on the free charges. For a free charge q , the force is $q\mathbf{E}$ and from the definition of ρ as charge density, we obtain the Coulomb force density $\rho\mathbf{E}$. The dielectric term represents the force on the dipoles. The dielectric term in (15) can be rewritten as $-\frac{1}{2} E^2 \nabla \varepsilon = -\nabla \left(\frac{1}{2} (\varepsilon - \varepsilon_0) E^2 \right) + (\varepsilon - \varepsilon_0) (\mathbf{E} \cdot \nabla) \mathbf{E}$, taking into account $(\mathbf{E} \cdot \nabla) \mathbf{E} = \nabla E^2 / 2$ for irrotational fields. For an incompressible fluid, the first term on the right-hand side can be incorporated into the pressure. The

second term, $(\varepsilon - \varepsilon_0)(\mathbf{E} \cdot \nabla)\mathbf{E} = (\mathbf{P} \cdot \nabla)\mathbf{E}$, represents the force density on n dipoles per unit volume, taking into account the force on an individual dipole \mathbf{p} as $(\mathbf{p} \cdot \nabla)\mathbf{E}$ and the definition of the polarization vector as $\mathbf{P} = n\mathbf{p}$.

The dielectric force in a homogeneous fluid (spatially constant properties) does not produce continuous flow; its influence is important in the hydrostatic equilibrium [18]. The dielectric siphon is a good example of how liquid flow can be achieved with dielectric forces [18]. However, the dielectric siphon is not a pump that can move fluid in a loop or between two points at equal pressure. The term responsible for generating pumping in Electrohydrodynamics is primarily the Coulomb force $\rho\mathbf{E}$. There are three main mechanisms of generating free charge in the bulk of a dielectric liquid: (a) injection of ions in a very insulating liquid from electrodes; (b) generation of nonequilibrium layers of free charge close to the electrodes because the rate of dissociation of neutral molecules exceeds the rate of recombination of ions [3]; and (c) induction of charges in a conducting liquid due to gradients of electrical conductivity. These three mechanisms give rise to three kinds of pumps.

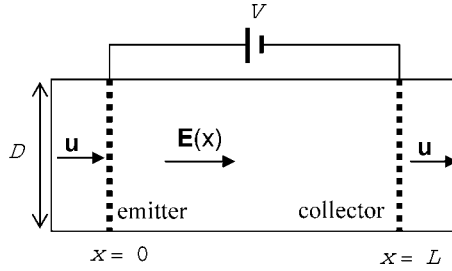


Fig. 1. Injection pump configuration

2.1. Injection Pump

The injection pump, also known as ion-drag pump, uses the interaction of an electric field with electric charges injected into a dielectric fluid. The electric field is imposed between an electrode called emitter and another called collector. The ions, travelling from the emitter to the collector, drag by friction the working fluid.

This pumping mechanism has been known for quite some time. Stuetzer [19, 20] and Pickard [21, 22] were among the first who studied theoretically and experimentally this EHD pump. In microsystems, Richter and coworkers [2, 23] fabricated an ion-drag EHD micropump, consisting

of pairs of metallic planar grids through which the pumped fluid moves. Ahn and Kim [24] experimented with an ion-drag pump that consisted of pairs of coplanar microelectrodes. Darabi et al. [25] tested different designs of coplanar microelectrodes for ion-drag pumping: emitter electrodes of planar shapes, of saw-tooth shapes or of saw-tooth shapes with bumps.

2.1.1. Pump Principle

Let us consider two plane-parallel perforated electrodes placed perpendicular to the axis of a pipe of circular cross section along which the liquid is pumped (see Fig. 1). For instance, this is a first approximation of two parallel wire grids that function as emitter and collector [2]. The emitter supplies ions that are driven by the electric field toward the collector placed at a distance L from the emitter. We restrict here to the simple case of unipolar injection (only one kind of ion is present). The body force applied to the liquid is the Coulomb force $\mathbf{f} = \rho\mathbf{E}$. As a simplification, we are going to consider the problem one-dimensional. The force per unit area generated by the pump is

$$\Delta p = \int_0^L \rho E \, dx. \quad (16)$$

From the Gauss's law in this 1D-problem, i.e. $\partial \varepsilon E / \partial x = \rho$,

$$\Delta p = \int_0^L \frac{\partial \varepsilon E}{\partial x} E \, dx = \frac{\varepsilon E_L^2}{2} - \frac{\varepsilon E_0^2}{2}, \quad (17)$$

where $E_L = E(L)$ is the field at the collector and $E_0 = E(0)$ is the field at the emitter. The 1D current density is, neglecting diffusion,

$$j = \rho(\mu E + u) = (\mu E + u) \frac{\partial \varepsilon E}{\partial x}. \quad (18)$$

In this simplified 1D-problem, the fluid velocity u is the average velocity in a cross section of the pipe. In the steady state, the current density and fluid velocity are constant along x . Equation (18) can be integrated and the electric field strength is

$$E = \left[\frac{2jx}{\varepsilon\mu} + \left(E_0 + \frac{u}{\mu} \right)^2 \right]^{1/2} - \frac{u}{\mu}. \quad (19)$$

The charge density is

$$\rho = \frac{j/\mu}{\left[\left(E_0 + u/\mu \right)^2 + 2jx/\varepsilon\mu \right]^{1/2}}. \quad (20)$$

Here $u > 0$, the liquid moves in the same direction as the ions, which is the case when the flow is generated by the pump. From the emitter to the collector, the charge density decreases while the field strength E increases. The injection of charge decreases the electric field at the emitter, since each additional unipolar charge already present in the pipe repels the incoming charge. When the field is too low, charge can no longer be removed from the emitter, and the pump reaches its space charge limit [26].

Let us analyse first the case when the fluid velocity is much smaller than the ion-migration velocity, $u \ll \mu V/L$. For space-charge-limited emission (SCLE), the electric field at the emitter is much smaller than the average field, $E_0 \ll V/L$. The boundary condition is, therefore, $E_0 \approx 0$. This happens under strong injection, $\rho \rightarrow \infty$ at the emitter. In this case, the generated pressure is maximized because $E_0 \approx 0$, see Eq. (17). The electric field is

$$E(x) = \left[\frac{2jx}{\varepsilon\mu} \right]^{1/2}. \quad (21)$$

From $V = \int_0^L E \, dx$, the current density can be obtained,

$$j = \frac{9}{8} \frac{\mu \varepsilon V^2}{L^3} \quad (22)$$

and the generated pressure is

$$\Delta p_{\max} = \frac{9}{8} \frac{\varepsilon V^2}{L^2}. \quad (23)$$

Under these conditions, the maximum average fluid velocity and flow rate that the pump can deliver are

$$u_{\max} = \frac{9}{8} \frac{\varepsilon V^2}{L^3} \frac{D^2}{32\eta} \quad Q_{\max} = \frac{9}{8} \frac{\varepsilon V^2}{L^3} \frac{\pi D^4}{128\eta}, \quad (24)$$

where D is the diameter of the pipe. Here we have used expression (13) since laminar flow is expected to be valid in microsystems.

For the dynamic case ($u \neq 0$) and under SCLE condition, $E_0 = 0$, the equations provide voltage and generated pressure as functions of u and j [19]:

$$V = \frac{\varepsilon\mu}{3j} \left\{ \left[\frac{2jL}{\varepsilon\mu} + \left(\frac{u}{\mu} \right)^2 \right]^{3/2} - \left(\frac{u}{\mu} \right)^3 \right\} - \frac{uL}{\mu}, \quad (25)$$

$$\Delta p = \frac{\varepsilon}{2} \left\{ \left[\frac{2jL}{\varepsilon\mu} + \left(\frac{u}{\mu} \right)^2 \right]^{1/2} - \frac{u}{\mu} \right\}^2. \quad (26)$$

Voltage drop and current density can be expressed as functions of the generated pressure Δp and flow velocity u

$$j = \frac{\varepsilon\mu}{2L} E_L \left[E_L + \frac{2u}{\mu} \right], \quad (27)$$

$$V = \frac{2L}{3} E_L \frac{E_L + \frac{3}{2}u/\mu}{E_L + 2u/\mu}, \quad (28)$$

where $E_L = \sqrt{2\Delta p/\varepsilon}$. The generated pressure by the pump is used in overcoming the internal hydrodynamic resistance of the pump plus the external load: $\Delta p = R_{in}Q + \Delta p_{out}$, where $R_{in} = 128\eta L/\pi D^4$. It is now possible to obtain the flow rate Q versus the external back pressure Δp_{out} at different applied potentials V . Here we can see that if ion migration velocity μE_L is much smaller than the fluid velocity u , the voltage drop is $V = E_L L/2$ and the pressure generated is $\Delta p = 2\varepsilon V^2/L^2$. Therefore, the maximum pressure at negligible flow rate and the maximum flow rate at zero pressure are, respectively,

$$\Delta p_{max} = 2\varepsilon V^2/L^2 \quad Q_{max} = 2\varepsilon V^2/(R_{in}L^2), \quad (29)$$

which are 16/9 times greater than for the case $u \ll \mu E$.

Up to here the theory has taken into consideration that there is only one kind of charge, i.e. unipolar injection. In practice, there are always other

ions different from those injected that come from dissociation of impurities or of the liquid itself. All these ions should be considered when dealing with a real experiment. According to Pickard [21] dissociation will produce equal amounts of positive and negative ions and their contribution to the space charge should be negligible. The pressure heads can be relatively well accounted for by emission theory, while the total current is not so well explained. This is because the electric force comes from the space charge originated by emission processes, while the measured current is the sum of the emission current and the conduction current.

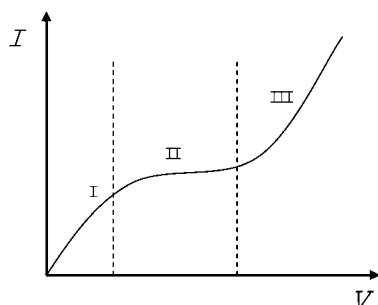


Fig. 2. Typical current-versus-voltage characteristic for a dielectric liquid

The current-versus-voltage characteristic for a dielectric liquid will typically have a form as shown in Fig. 2 [9,13]. Generally, different behaviors can be distinguished. At low voltages (region I), the current is caused by the dissociation of impurities in the liquid, and ohmic behavior is observed. As the voltage increases (electric fields around 10^5 V m^{-1}), ions generated by the dissociation of impurities can not be created as fast as they are neutralized at the electrodes and the current density reaches saturation (region II). This region II is always present in gases but is ill-defined or may not be present in dielectric liquids. At higher voltages, a steep increase in the current is observed (region III). The beginning of region III can be due to enhancement of the dissociation process of impurities by the electric field strength. Nevertheless, at further increase of the electric field strength, ion injection from the electrodes becomes the dominating process. The current then tends to the $I \propto V^2$ law of the space-charge-limited emission. Finally, at electric fields of sufficient high strength (of the order of 100 MV m^{-1}), breakdown may take place. The breakdown electric field is very dependent on the liquid, impurities, and geometry.

To reduce the voltage needed to observe the emission, the emitter is usually designed to produce a local, highly intense electric field. The emitters usually have sharp edges or points while the collectors should be as smooth as possible. For instance, in the ion-drag pump experiments using arrays of coplanar microelectrodes by Darabi et al. [25], the micropump with saw-tooth-shaped emitters with bumps obtained the best pumping performance.

2.1.2. Characteristics

2.1.2.1. Efficiency

According to Crowley et al. [26], the electrical power consumption of the ion-drag pump, which is the product of voltage and current, can be approximated by

$$P_{\text{in}} = jSV \sim \rho(u + \mu E)SV + \sigma ESV, \quad (30)$$

where S is cross-sectional area, and E and ρ are here the mean electric field and mean charge density, respectively. The term σE is the ordinary bipolar conduction, in which charge carriers are not produced by injection but by dissociation of impurities in the bulk. We may think of this as residual currents that do not contribute to the pumping. Crowley et al. defined the useful output power of the pump as all the mechanical work, rather than the mechanical work the pump delivers to a external load. Under this consideration, the output power is $P_{\text{out}} \sim \rho EuSL = \rho uSV$, giving an efficiency of

$$\text{eff}^* = \frac{P_{\text{in}}(\mu = \sigma = 0)}{P_{\text{in}}} = \frac{1}{1 + \alpha}, \quad (31)$$

where α is the coefficient,

$$\alpha = \frac{\mu E}{u} + \frac{\sigma E}{\rho u}. \quad (32)$$

From our definition of efficiency, (14), we obtain $\text{eff} \sim \text{eff}^*/4$, considering $Q_{\text{max}} = u_{\text{max}}S$ and $\Delta p_{\text{max}} \sim \rho EL$. The absolute maximum efficiency is $\text{eff} = 0.25$, when $\alpha = 0$, which can also be obtained from the values of maximum pressure and flow rate given in (29). Since $\alpha = 0$ implies that the ion mobility must vanish, the pump is more efficient if the fluid velocity is much greater than the ion-migration velocity μE .

The second term due to the losses originated by residual conductivity can be written as

$$\frac{\sigma E}{\rho u} \sim \frac{L/u}{\varepsilon/\sigma}, \quad (33)$$

where the charge density estimate $\rho \sim \varepsilon E/L$ comes from Gauss's law. It can be seen that the expression is the ratio of two characteristic times: the numerator is the transit time and the denominator is the charge relaxation time of the fluid. For high efficiency, this ratio should be small, i.e., the fluid must go from emitter to collector before the charge has time to relax.

The maximum efficiency obtained in the experiments of Darabi and Wang [27] was around 0.0015 for an applied voltage of 180 V using refrigerant HFE-7100 as working fluid.

2.1.2.2. Liquids

Typically, the liquids that are candidate to be pumped by ion-drag micropumps are highly insulating liquids. An upper bound for the conductivity of the liquid to be pumped comes from comparison between the time needed for the ion to go from the emitter to the collector and the charge relaxation time ε/σ . If the charge relaxation time is too short, the charge is screened before enough force is transmitted to the liquid. Therefore, we do not expect that ion-drag pumps can actuate liquids with conductivities $\sigma \gg v \varepsilon/L$, where v is the ion velocity $v = u + \mu E$. Crowley et al. [26] presented a table of liquids that were good candidates to be used as working fluids for ion-drag pumps. The highest conductivity in that table of liquids was around 10^{-7} S m^{-1} . In microsystems, Richter and Sandmaier [2] were able to pump several organic solvents such as ethanol, methanol, acetone, and propanol. Richter et al. [23] and Ahn and Kim [24] presented results with ethanol as working fluid, which, according to Crowley et al. [26], has a conductivity around 10^{-7} S m^{-1} if it is not deionized. The liquids used in the micropump of Darabi and Wang [27] had conductivities lower than 10^{-9} S m^{-1} . The highest fluid velocities are predicted for liquids with high dielectric constant and low viscosity. However, high dielectric constant also means that they have conductivities too large to allow efficient operation. Liquids of high dielectric constant should be deionized, in order to be used for ion-drag pumping.

2.1.2.3. Problems

The high electric field strengths used can change the liquid electrical properties, and can cause corrosion of the electrodes. These two effects can affect run-to-run repeatability and reduce pump life. However, some liquids like liquid nitrogen can be ideal working fluids for ion drag pumping. According to Darabi and Wang [27] slight electrode degradation was observed using the HFE-7100 fluid; however, no noticeable electrode degradation was observed using liquid nitrogen. It seems that the good performance of liquid nitrogen is due to its very stable molecular structure. According to Zhakin [13], the choice of a liquid, electrode material, and ionizing groups can be important in order to have reproducible results.

2.1.2.4. Applications

A potential application of an ion-drag pumping system is its use in pumping fluids in cryogenic cooling microsystems. Cryogenic cooling has become a widely adopted technique to improve the performance of electronics and sensors. Super-conducting devices, which are used to increase signal-to-noise ratio in communications, must also be maintained at cryogenic temperatures. Micropumps capable of pumping liquid nitrogen would enable the development of compact and lightweight chip-integrated cooling systems [27, 28]. In [28], the tested micropumps were able to pump sufficient liquid nitrogen to cool super-conducting sensors and detectors in a cryogenic chamber.

Other promising applications for ion-drag micropumps include fuel injection loops, and gas and liquid pumping where small quantities of dielectric fluids need to be pumped.

2.2. Conduction Pump

Under the weak electric field regime (field much less than 10^7 V m^{-1}), the conduction in a dielectric liquid is carried out by ions generated by dissociated molecules. When an electric field exceeds a certain threshold (on the order of 10^5 V m^{-1}), there appear layers in the vicinity of the electrodes where the rate of dissociation exceeds that of the recombination. These nonequilibrium layers are charged, with the opposite sign from that of the adjacent electrode [3, 29]. The thickness of these heterocharge layers is much greater than the Debye length and increases with the electric field. The Coulomb force acting on these charge layers produce the pumping mechanism. Because the thickness of the charge layer is much

greater than the Debye length, we have included this kind of pump among those whose mechanism is due to electric forces in the bulk.

Micropumps based on conduction EHD pumping have not yet been reported, although Atten and Seyed-Yagoobi [3] and Jeong and Seyed-Yagoobi [30] reported conduction EHD pumps in the centimeter scale.

2.2.1. Pump Principle

The EHD conduction pumping mechanism can be illustrated considering two parallel perforated electrodes immersed in a dielectric liquid [3, 31]. The analysis here presented considers that no injection from electrodes takes place (the ions reaching the electrodes neutralize). Electric conduction in a pure dielectric liquid can be explained with a simple model, which considers a reversible process of dissociation-recombination of a neutral species (denoted by AB) into univalent positive A^+ and negative B^- ions. These ions are the charge carriers between the parallel electrodes.

Let us assume that the electrode placed at $x = 0$ is subjected to a potential V and the electrode placed at $x = L$ is grounded (geometry as in Fig. 1). The governing 1D-equations for the steady-state behavior of the ionic and neutral species are

$$\frac{\partial \mu_+ n_+ E}{\partial x} = k_d n_0 - k_r n_+ n_-, \quad (34)$$

$$\frac{\partial \mu_- n_- E}{\partial x} = -k_d n_0 + k_r n_+ n_-, \quad (35)$$

and

$$\frac{\partial E}{\partial x} = e \frac{n_+ - n_-}{\varepsilon}, \quad (36)$$

where k_d and k_r denote the dissociation and recombination rates, respectively. Several assumptions are made: (a) the dissociation rate is very small so that the neutral species concentration n_0 is constant and (b) diffusion and convection are neglected. At equilibrium $k_d n_0^{\text{eq}} = k_r n_+^{\text{eq}} n_-^{\text{eq}}$ and $n_+^{\text{eq}} = n_-^{\text{eq}} = n^{\text{eq}}$.

The boundary conditions for the previous equations are the following:

(a) $n_+ = 0$ at $x = 0$ and $n_- = 0$ at $x = L$, because of the Coulomb

repulsion between electrode and co-ions and (b) $\int_0^L E(x) dx = V$, where V is the applied potential difference between electrodes. These equations were solved by Thomson and Thomson [32]. They provided an approximate solution valid for the quasi-ohmic regime, i.e., when the thickness of the heterocharge layer, λ , is much smaller than the distance between electrodes L . In this case, the liquid is electroneutral in the bulk except for the heterocharge layers. The approximation consists on neglecting the recombination in the heterocharge layers. For the layer adjacent to the positive electrode ($x = 0$), the approximate solution for $x \leq \lambda_+$ is

$$\mu_+ n_+ E = k_d n_0 x. \quad (37)$$

The electric current is constant along x

$$\sigma E_b = e(\mu_+ n_+ + \mu_- n_-)E = ek_d n_0 x + e\mu_- n_- E, \quad (38)$$

where E_b is the electric field in the bulk and $\sigma = e(\mu_+ + \mu_-)n^{\text{eq}}$ is the bulk conductivity. For $x > \lambda_+$, the liquid is assumed to be electro-neutral, $n_+ = n_- = n^{\text{eq}}$. The thickness λ_+ can be obtained from $\sigma E_b = ek_d n_0 \lambda_+ + e\mu_- n^{\text{eq}} E_b$ giving

$$\lambda_+ = \frac{\mu_+ n^{\text{eq}} E_b}{k_d n_0} = \frac{\mu_+ E_b}{k_r n^{\text{eq}}}. \quad (39)$$

Equivalently, for the charge layer adjacent to the negative electrode,

$$\lambda_- = \frac{\mu_- E_b}{k_r n^{\text{eq}}}. \quad (40)$$

The thickness of the charge layer can be seen as the distance that an ion, under the action of the electric field, travels without recombination, taking into account that $t_c = 1/k_r n^{\text{eq}} \approx \varepsilon/\sigma$ [33] is the charge relaxation time.

Solving Gauss's law in the charge layer $0 \leq x \leq \lambda_+$ leads to [34]

$$E = E_b \sqrt{1 + (1 - x/\lambda_+)^2 \mu_+/\mu_-}. \quad (41)$$

The value of the electric field in the bulk is close to V/L for $\lambda_+/L \ll 1$ and $\lambda_-/L \ll 1$, typically, when $\varepsilon V/en^{\text{eq}}L^2 \ll 1$.

In the two charge layers, the Coulomb force is directed towards the electrodes. In the absence of motion, the force balance equation gives

$$\frac{\partial p}{\partial x} = e(n_+ - n_-)E = \frac{\partial \varepsilon E}{\partial x} E = \frac{\partial \varepsilon E^2/2}{\partial x}. \quad (42)$$

Therefore, the pressure generated in the layer close to $x = 0$ is

$$p_0 - p_b = \frac{\varepsilon}{2}(E_0^2 - E_b^2) = \frac{\varepsilon}{2}E_b^2 \frac{\mu_+}{\mu_-}, \quad (43)$$

where p_0 is the pressure at $x = 0$ and p_b is the pressure in the bulk. An equivalent expression can be obtained for the pressure drop across the layer adjacent to the negative electrode:

$$p_b - p_L = \frac{\varepsilon}{2}(E_b^2 - E_L^2) = -\frac{\varepsilon}{2}E_b^2 \frac{\mu_-}{\mu_+}, \quad (44)$$

where p_L is the pressure at $x = L$. The total pressure generated across the pump is, therefore,

$$p_0 - p_L = \frac{\varepsilon}{2}E_b^2 \left(\frac{\mu_+}{\mu_-} - \frac{\mu_-}{\mu_+} \right). \quad (45)$$

Here, contrary to [3, 31], the net pressure is different from zero because of the difference in mobilities between positive and negative ions.

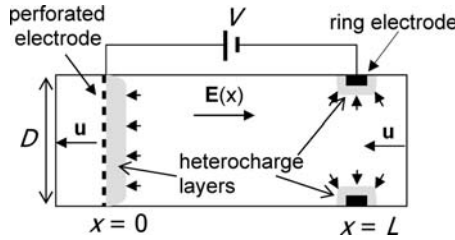


Fig. 3. Scheme of the conduction pump of ref. [31]

To have a pressure difference even in the case of equal mobilities, the electrode pair is made nonsymmetric [3, 30, 31]. For instance, a perforated disc electrode against a ring electrode was used in [31] (see Fig. 3). The Coulomb force in the charge layer adjacent to the perforated disc electrode is mainly axial while the electric force in the charge layer adjacent to the ring electrode is mainly radial. The radial force is balanced by the pipe

wall while the axial force drives the dielectric liquid along the pipe. According to [31], the pressure generated at zero flow rate for this configuration is $\Delta p_{\max} = 0.85\varepsilon V^2/L^2$, which is of the order of the expressions previously obtained for only one electrode, (43). For finite flow rate, if the convection current can be neglected in front of the conduction current, the previous expression for the maximum pressure is the total force per unit area that the pump exerts to the fluid. In this case, the maximum average fluid velocity and flow rate that this pressure can generate are

$$u_{\max} = 0.85 \frac{\varepsilon V^2}{L^3} \frac{D^2}{32\eta} \quad Q_{\max} = 0.85 \frac{\varepsilon V^2}{L^3} \frac{\pi D^4}{128\eta}. \quad (46)$$

Experimentally, the conduction pump drives the liquid in the opposite direction as the ion-drag pump for the same geometry. For instance, in the point-plane configuration of [3], the liquid moves towards the point in the low voltage regime (below 17.5 kV) and moves from the point to the plane for higher voltages. This indicates that in this geometry the effect of direct injection of charges overcomes the corresponding effect of the heterocharge layers at approximately 17.5 kV.

2.2.2. Characteristics

2.2.2.1. Efficiency

For $\lambda \ll L$, we can estimate the electric input power $IV \approx \sigma V^2 S/L$. The energy efficiency is then

$$eff = \frac{\Delta p_{\max} Q_{\max}}{4IV} \approx 0.2 \frac{u_{\max} \varepsilon}{\sigma L} \approx 0.2 \frac{\varepsilon^2 V^2 D^2}{32 L^4 \eta \sigma}. \quad (47)$$

The combination of parameters $u\varepsilon/\sigma L$ is called the electric Reynolds number [35]. It represents the ratio between convection current and conduction current. In the conduction regime, the convection of current is usually negligible, so that this number is typically very small. The efficiency decreases as σ increases. For the experiments presented in [31] at $V = 10$ kV, the maximum efficiency was $eff \sim 10^{-3}$.

2.2.2.2. Liquids

Liquids of low conductivity can be used as working fluids. An upper bound for σ comes from the thickness of the heterocharge layer as compared to the Debye length. If the conductivity is high, both layers

(diffuse and heterocharge layers) can have similar thicknesses. In this case, the diffusion processes are not negligible and the approximations are not applicable. This condition $\lambda \gg \lambda_D$ implies that the conductivity should be $\sigma \ll \mu \epsilon e E^2 / k_B T$. A lower bound for σ comes from the comparison between the heterocharge layer thickness λ and the distance between electrodes L [3]. If $\lambda \gg L$, the recombination is negligible also in the bulk. This gives rise to the saturation regime for the current where the ions are removed from the bulk at the rate of production. In this situation, the electric current increases very slightly with voltage approaching the asymptotic value $j_{\text{sat}} = e k_d n_0 L$. The electric field does not vary significantly between electrodes [34] and the pressure generated is small (because the pressure comes from the increments in ϵE^2). Therefore, in order to have significant pressure, the conductivity should not be much smaller than $\mu E \epsilon / L$. In [3], the pressure obtained for the working liquid n-hexane was smaller than predicted ($\sigma = 7 \times 10^{-11} \text{ S m}^{-1}$). For this liquid, the authors estimated $\lambda \sim 4L$ ($C_0 \sim 0.25$ in their notation), and the conclusion was that the pressure generated will take much smaller values than the prediction $\Delta p_{\text{max}} \sim \epsilon V^2 / L^2$ when $\lambda \gg L$. Tentatively, we can say that a lower bound for σ is $0.01 \mu E \epsilon / L$. Therefore, the conduction pump will mainly operate for liquids with conductivities between

$$0.01 \frac{\mu \epsilon V}{L^2} < \sigma < \frac{\mu \epsilon V}{L^2} \frac{e V}{k_B T}. \quad (48)$$

In [3, 30, 31], the primary working fluid was HCFC refrigerant R-123 with conductivity $\sigma = 2.8 \times 10^{-8} \text{ S m}^{-1}$, which is greater than $\mu \epsilon V / L^2 \sim 10^{-9} \text{ Sm}^{-1}$ for their experimental conditions.

2.2.2.3. Problems

The voltages can not exceed the threshold voltage for charge injection, which may limit the pressure and flow generated. To limit the charge injection, the use of electrodes with small radii of curvature should be avoided. As an advantage, the working fluid and electrodes are not subjected to the degradation that ion injection usually generates.

2.2.2.4. Applications

As for the ion-drag pump, the main application may be the pumping of refrigerant for chip-integrated cooling systems.

2.3. Induction Pump

In this pump, charge is induced in an inhomogeneous liquid by the electric field, and the electric force upon this induced charge is transmitted to the liquid. Usually the inhomogeneity in the liquid is achieved by imposing a gradient of temperature. Liquid conductivity depends on temperature mainly because ionic mobilities are inversely proportional to viscosity (that depends on temperature) and because the dissociation rate of neutral molecules also depends on temperature. The common induction pump consists of an array of coplanar electrodes subjected to a travelling wave potential together with a vertical gradient of temperature (see Fig. 4) [36]. The temperature gradient may be obtained by the Joule heating generated by the imposed electric field instead of by an externally imposed temperature gradient. Typically, this has been the case in the application of this pump in microfluidics [4, 37, 38]. Recently, an induction pump was realized that employs an external gradient of temperature [39]. Unidirectional motion can also be obtained with an array of electrodes subjected to a single phase signal with an imposed longitudinal temperature gradient [40, 41].

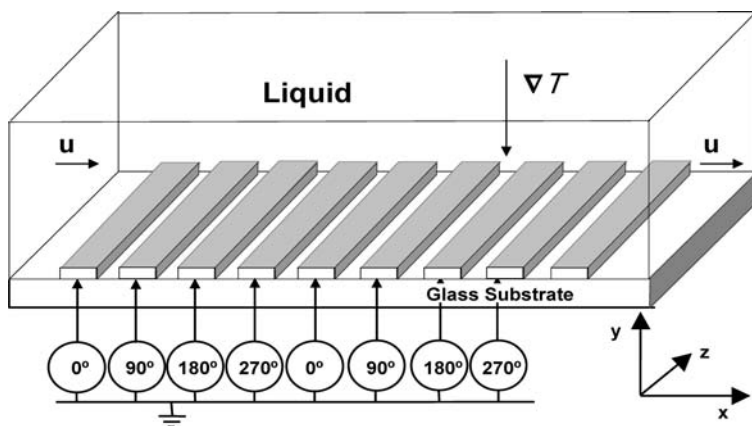


Fig. 4. Scheme of travelling wave induction pump

2.3.1. Pump Principle

Let us consider a simple geometry like the one shown in Fig. 1: two parallel perforated electrodes subjected to a potential difference inside a circular capillary. The electrode at $x = 0$ is at temperature T_0 and the electrode at $x = L$ is at temperature T_L . Solving the diffusion equation for temperature, a linear temperature profile is achieved between electrodes in the steady state. Because the conductivity and permittivity of the liquid are functions of T , gradients of conductivity and permittivity will appear. The increment of temperature between electrodes is such that, in good approximation, there are also linear variations for σ and ε between the electrodes:

$$\sigma(x) = \sigma_1 + ax \quad \varepsilon(x) = \varepsilon_1 + bx. \quad (49)$$

where a and b are given by

$$a = \frac{d\sigma}{dT} \frac{dT}{dx} \quad b = \frac{d\varepsilon}{dT} \frac{dT}{dx}. \quad (50)$$

We assume that any convection of current is negligible in front of the conduction of current. In this case the continuity of current leads to

$$\frac{\partial \sigma E}{\partial x} = 0 \quad j = \sigma E = \text{constant}. \quad (51)$$

And from $\int_0^L E dx = V$ we obtain

$$j = V \left(\int_0^L \frac{dx}{\sigma} \right)^{-1} = \frac{aV}{\ln(1 + aL/\sigma_1)}. \quad (52)$$

An induced charge density appears in the bulk

$$\rho = \frac{\partial \varepsilon E}{\partial x} = \sigma E \frac{\partial}{\partial x} \left(\frac{\varepsilon}{\sigma} \right) = E \frac{\sigma b - \varepsilon a}{\sigma}. \quad (53)$$

In this case that the permittivity varies spatially, the electric force expression has two contributions, the Coulomb term and the dielectric term

$$f = \rho E - \frac{1}{2} E^2 \frac{\partial \varepsilon}{\partial x} = E \frac{\partial \varepsilon E}{\partial x} - \frac{1}{2} E^2 \frac{\partial \varepsilon}{\partial x} = \frac{1}{2} \frac{\partial \varepsilon E^2}{\partial x}. \quad (54)$$

The pressure drop that is generated at zero flow rate is then

$$\Delta p_{\max} = \frac{1}{2} \varepsilon(L) E^2(L) - \frac{1}{2} \varepsilon(0) E^2(0) = \frac{j^2}{2} \left(\frac{\varepsilon(L)}{\sigma(L)^2} - \frac{\varepsilon(0)}{\sigma(0)^2} \right). \quad (55)$$

For the case $bL/\varepsilon_1 \ll 1$ and $aL/\sigma_1 \ll 1$ the pressure drop is

$$\Delta p_{\max} = \frac{1}{2} \varepsilon_1 \frac{V^2}{L^2} \left(\frac{bL}{\varepsilon_1} - \frac{2aL}{\sigma_1} \right) = \frac{1}{2} \varepsilon_1 \frac{V^2}{L^2} (\beta - 2\alpha)(T_L - T_0), \quad (56)$$

where $\alpha = (1/\sigma)(d\sigma/dT)$ and $\beta = (1/\varepsilon)(d\varepsilon/dT)$. For water-saline solutions, $\alpha \sim 0.02 \text{ K}^{-1}$ and $\beta \sim -0.004 \text{ K}^{-1}$. If $T_0 > T_L$ the pump drives the fluid from $x = 0$ to $x = L$, as should be for a positive induced charge (see (53)). The liquid motion modifies the linear profile of temperature because of heat convection. To neglect heat convection in front of heat diffusion, the Péclet number should be small, i.e. $uL/\chi < 1$, where χ is the thermal diffusivity. It can be seen, by solving the 1D convection-diffusion equation for temperature, that the linear profile is not very much distorted even if $uL/\chi = 1$. For a fluid velocity of 1 mm s^{-1} , length $L = 10^{-4} \text{ m}$ and water thermal diffusivity $\chi = 1.4 \times 10^{-7} \text{ m}^2 \text{ s}^{-1}$, the Péclet number is close to 0.7, and the previously calculated expressions for T and Δp are approximately correct. Assuming that the convection of temperature and the convection of charge are negligible, the maximum average fluid velocity and flow rate that this pressure can generate are

$$u_{\max} = \frac{1}{2} \frac{\varepsilon_1 V^2}{L^3} \frac{D^2}{32\eta} (2\alpha - \beta)(T_0 - T_L) \quad Q_{\max} = u_{\max} \frac{\pi D^2}{4}. \quad (57)$$

With these simple expressions, we can see that the induction pump generates much smaller flow rate and pressure than the conduction or injection pumps for the same applied voltage and geometry (between 5 and 10 times less). In effect, the temperature increment will be on the order of 10 K or less, and the pressure generated is on the order of $\Delta p \sim \varepsilon(V^2/L^2)\alpha\Delta T \leq 0.2\varepsilon(V^2/L^2)$ in the case of water.

To avoid faradaic reactions, AC voltages of high enough frequency should be applied. In this case, the time-average force is different from zero because it is quadratic with voltage. The expressions are the same substituting V by the rms value V_{rms} . The theoretical results presented here are valid in the AC case if the angular frequency of the applied signal ω is much smaller than σ/ε . For frequencies $\omega \gg \sigma/\varepsilon$, the liquid behaves as a pure dielectric liquid and no free charge is induced. However, the dielectric force is still operating at these frequencies, giving a generated

pressure of the order of $\Delta p \sim \varepsilon(V^2/L^2)\beta\Delta T$, which is α/β times smaller than the force for $\omega \ll \sigma/\varepsilon$ (around 5 times smaller if the liquid is water).

As already mentioned, the usual experimental case (see Fig. 4) consists of an array of coplanar electrodes subjected to a travelling wave signal $V_0 \cos(\omega t - kx)$ and to a vertical gradient of temperature that is generated by Joule heating [4]. In this case, the vertical component of the electric field induces free charge in the liquid bulk, while the longitudinal component acts on the induced charge driving the liquid along the array. The dependence of the electric force with frequency is very different from the case we have just analysed. Here, the force is maximized at $\omega = \sigma/\varepsilon$, going to zero at high and low frequencies. For a long channel of rectangular cross section (where h is the height, w the width and $w \gg h$), the expressions for the average velocity and flow rate at zero pressure can be obtained from the results of [36]

$$u_{\max} = \frac{\varepsilon V_0^2}{16h\eta} (\alpha - \beta) \Delta T \frac{\omega\tau}{1 + (\omega\tau)^2} \quad Q_{\max} = u_{\max} hw, \quad (58)$$

where $\tau = \varepsilon/\sigma$ is the charge relaxation time of the liquid and ΔT is the temperature difference between top and bottom of the channel. Here it was supposed that $kh \gg 1$ and that the change in permittivity and conductivity are small, $\Delta\varepsilon/\varepsilon \ll 1$ and $\Delta\sigma/\sigma \ll 1$. The pressure that can be generated per wave-length $L = 2\pi/k$ is

$$\Delta p_{\max} = \frac{12\eta u L}{h^2} = \frac{3}{4} \frac{\varepsilon V_0^2 (\alpha - \beta) \Delta T L}{h^3} \frac{\omega\tau}{1 + (\omega\tau)^2}. \quad (59)$$

If $L \sim h \sim w$, these expressions for Δp_{\max} and Q_{\max} at frequency $\omega = 1/\tau$ are of the same order as the previously obtained expressions (56, 57).

When the origin of the temperature gradient is due to Joule heating, the boundary conditions for the temperature are essential in order to know the generated velocity or pressure. Nevertheless, an estimation of the increment of temperature can be obtained from the temperature equation neglecting heat convection [42]

$$\sigma E^2 + \kappa \nabla^2 T = 0, \quad (60)$$

where κ is thermal conductivity. The estimate for the increment of temperature is $\Delta T \sim \sigma V_{\text{rms}}^2 / \kappa$, which leads to pressure and flow proportional to V^4 when Joule heating governs the temperature profile.

2.3.2. Characteristics

2.3.2.1. Efficiency

The efficiency of the EHD induction micropump can be estimated as

$$eff = \frac{1}{4} \frac{\Delta p_{\max} Q_{\max}}{IV + \dot{q}}, \quad (61)$$

where \dot{q} is the power that is consumed in order to generate the temperature difference. When the temperature profile is generated by Joule heating, \dot{q} is already included in the term IV . For an imposed temperature gradient in the system of parallel electrodes studied before, the minimum value of \dot{q} should be $\dot{q} \sim Sk\Delta T/L$, where S is the area of the pipe and ΔT the difference of temperature between electrodes. For small increments of temperature ($\Delta\varepsilon/\varepsilon \ll 1$ and $\Delta\sigma/\sigma \ll 1$), the maximum energy efficiency is

$$eff \approx \frac{1}{4} \frac{(u_{\max} \varepsilon / \sigma L) \alpha \Delta T}{1 + \dot{q} / IV} \approx \frac{\varepsilon^2 V^2 D^2 (\alpha \Delta T)^2}{128 \sigma \eta L^4 (1 + \dot{q} / IV)}. \quad (62)$$

We can see that the efficiency is very small, proportional to the product of two small numbers: the electric Reynolds number and $\alpha \Delta T / (1 + \dot{q} / IV)$.

2.3.2.2. Liquids

The liquids that can be pumped should have some conductivity. In the previous expressions, the convection of charge was neglected in front of the ohmic current. This is a fair assumption when the electric Reynolds number is small $u\varepsilon/\sigma L \ll 1$ [35]. When the convection current is not small, the pattern of induced charge can be very different and the pump may not work. In addition, any charge that could be injected from the electrodes should relax in a distance much shorter than the typical length, i.e. $\mu E \varepsilon / \sigma L \ll 1$. Therefore, the condition is that the conductivity should be greater than $\sigma > v\varepsilon/L$, where $v = u + \mu E$. For a micropump where the velocity is $u \sim 10^{-3} \text{ ms}^{-1}$, typical length is $L \sim 10^{-5} \text{ m}$, the condition is $\sigma > 10^{-7} \text{ S m}^{-1}$ in the case of water, and $\sigma > 10^{-9} \text{ S m}^{-1}$ for non-polar liquids. An upper bound for σ comes from the generated temperature due to Joule heating. Typically the voltages needed to produce enough flow are in the range from 10 to 50 V peak-to-peak [38]. We expect that the increment of temperature will be excessive (reaching boiling temperature) for conductivities $\sigma \geq 1 \text{ S m}^{-1}$ [11]. Therefore, a wide range of conductivities can be used for this micropump: $10^{-9} < \sigma < 1 \text{ S m}^{-1}$.

2.3.2.3. Problems

If the electric field is very high, especially for liquids with conductivity around $\sigma \sim 1 \text{ S m}^{-1}$ or more, the temperature rise can be excessive. Also, this may be a limiting factor if we are interested in pumping liquids with bio-particles (cells, DNA,...) where the temperature must be controlled. The expected temperature rise for 0.1 S m^{-1} (0.01 S/m) at $V_0 = 10 \text{ V}$ is smaller than 10 K (1 K).

If the electric field is too high, there exists the possibility that EHD flow instabilities appear [36], destroying the pumping mechanism. The formation of gas bubbles is also a limiting factor at high electric fields, and especially at low frequencies. EHD instabilities and bubbles were observed at voltages around 40 V in the device studied in [38].

The problems related to the formation of bubbles by Faradaic currents can be eliminated by coating the electrodes with a thin dielectric layer. At high frequencies, the electric fields can penetrate the dielectric coating easily. As an advantage, avoiding Faradaic currents using dielectric coating makes the performance of the pump very reproducible: accurate pumping over eight months was observed in [38].

2.3.2.4. Applications

Since saline solutions with $\sigma < 1 \text{ S m}^{-1}$ can be pumped, the possible applications range from bio-medical to chemical analysis. To use the micropump for liquids with low conductivity, the temperature gradient should be imposed externally. The energy efficiency of this pump is low, nevertheless there are many applications where this is not a limiting issue. For example, we may have a macroscopic power generator to feed our microscopic device. Although the generated pressure is typically low, many applications do not require high pressure like the generation of secondary flows for mixing [43] or the generation of controlled circular streaming in microfluidic systems for cooling of special elements, or for supply of living cells.

3. Electric Forces in the Diffuse Layer: Electroosmotic and AC/IC Electroosmotic Pumps

At the interface between solid walls and electrolytes, double layers are formed [44] due to differences in electrochemical potentials of both phases. The solid surface becomes charged and counterions coming from the bulk liquid shield this surface charge. At equilibrium, the electrostatic

attraction between the charged surface and the counterions is balanced by thermal agitation. The liquid is electrically neutral except for a charged layer adjacent to the solid surface. The characteristic thickness of this layer is the Debye length, λ_D , given by

$$\lambda_D = \sqrt{\frac{\epsilon k_B T}{e^2 \sum_i z_i^2 n_i^\infty}}. \quad (63)$$

Here z_i and n_i^∞ are the valence number and number density of ionic species i in solution. For the case of a symmetric electrolyte, the Debye length can be written as $\lambda_D = \sqrt{\epsilon D / \sigma}$, where D is here the ion diffusion coefficient. The application of an electric field along the surface produces a Coulomb force on the diffuse charge and the liquid is set into motion. Because the thickness of the Debye layer is very small (1–100 nm in water) the Coulomb force is considered as a superficial force.

We can distinguish two ways of generation of charge at the solid surface: (a) a chemical mechanism such as ionization of bound surface groups or as ion adsorption and (b) an electrostatic mechanism in which the solid surface (typically a metal) gets charged because it is subjected to an electric potential difference with respect to the bulk electrolyte. In both cases, a double layer is formed in order to screen the charge of the solid surface. We can identify two kinds of pumps based on these charging mechanisms.

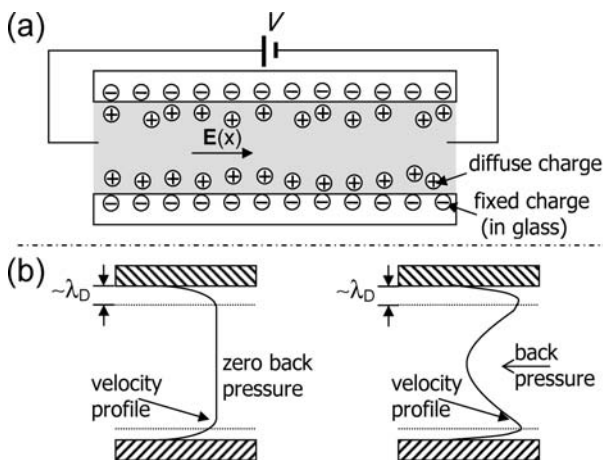


Fig. 5. Electroosmosis in a capillary. (a) The electric field acts on the counterions in the diffuse double layer. (b) Velocity profiles generated in the capillary with (right) and without (left) a back pressure

3.1. Electroosmotic Pump

A DC Electroosmotic (EO) pump makes use of the electric double layer that spontaneously develops between a liquid in contact with a solid. Generally, the chemical state of the solid surface is altered because of the presence of the electrolyte. For example, in the case of silica-based ceramics, like glass, with SiOH groups at the surface, a fraction of the Si–OH bonds change into Si–O– releasing the proton when immersed in water. It results in a net negatively charged surface. The resulting redistribution of ions in the liquid keeps the liquid bulk electrically neutral, while a positive diffuse charge layer appears close to the surface. Application of an electric field along the surface causes the mobile ions of the double layer to move towards the electrode of opposite sign dragging the fluid with them. In this case, bulk flow moves in the direction of the applied electric field. The negatively charged SiO– groups are bound to the solid surface by covalent bonds and hence will be stationary. Electroosmosis thus refers to the bulk movement of a liquid past a stationary solid surface due to externally applied electric field. The phenomenon is illustrated in Fig. 5.

The EO phenomena have been known for almost 200 years (F.F. Reuss discovered electroosmosis in 1809). Flows generated by EO pumping are used in a range of applications, including soil remediation or contaminant removal from groundwater, and have been used in chemical and biological analysis since a long time. Pretorius et al. [5] proposed electroosmosis for high-speed chromatography in 1974. A number of important techniques used in miniaturized systems for chemistry and life sciences make use of EO flow: flow injection analysis [45], on-chip electrophoretic separation [46], and on-chip liquid chromatography [47]. Yao and Santiago [48] presented a detailed description of the history and development of EO pumps that are able to generate high pressure.

3.1.1. Pump Principle

The most basic EO pump is simply a capillary or micro-pipe with electrodes submerged within end-channel reservoirs. Let us consider a cylindrical capillary of radius a [49], with the wall of the capillary at potential ζ , the zeta potential. Zeta potential is a key parameter in the theory of electrokinetics. Classical theory describes the electrical double layer as divided into the Stern layer and Gouy-Chapman diffuse layer [44]. The Stern or compact layer is formed of counterions absorbed onto the wall, while the ions of the Gouy-Chapman layer are diffuse. The plane

separating these two layers is called the shear plane, and the potential at this plane is the zeta potential.

Let us assume that inside the capillary there is a symmetric 1-1 electrolyte of bulk ionic concentration n^∞ . The Poisson-Boltzmann equation in this cylindrical geometry is

$$\frac{1}{r} \frac{\partial}{\partial r} \left(r \frac{\partial \Phi}{\partial r} \right) = -\frac{\rho(r)}{\varepsilon} = \frac{2en^\infty}{\varepsilon} \sinh \left(\frac{e\Phi}{k_B T} \right). \quad (64)$$

In the Debye-Hückel approximation [44], $e\Phi/k_B T \ll 1$, and the Poisson-Boltzmann equation becomes

$$\frac{1}{r} \frac{\partial}{\partial r} \left(r \frac{\partial \Phi}{\partial r} \right) = \frac{\Phi}{\lambda_D^2}, \quad (65)$$

where the Debye length is $\lambda_D = \varepsilon k_B T / 2e^2 n^\infty$. The general solution for this equation, which is finite at $r = 0$, is $\Phi(r) = AI_0(r/\lambda_D)$, where I_0 is the zero-order modified Bessel function of the first kind. Taking into account the boundary condition at $r = a$, the expressions for Φ and ρ are

$$\Phi(r) = \zeta \frac{I_0(r/\lambda_D)}{I_0(a/\lambda_D)} \quad \rho = -\frac{\varepsilon}{\lambda_D^2} \Phi. \quad (66)$$

Under an applied electric field in the axial direction, E_z , the free charge is subjected to a Coulomb force. The equation of liquid motion for an infinite cylindrical tube under the influence of an axial applied electric field and no applied pressure gradient is

$$\frac{\eta}{r} \frac{\partial}{\partial r} \left(r \frac{\partial u}{\partial r} \right) + E_z \rho = 0. \quad (67)$$

With the boundary no-slip condition $u(a) = 0$,

$$u(r) = -\frac{\varepsilon \zeta E_z}{\eta} \left(1 - \frac{I_0(r/\lambda_D)}{I_0(a/\lambda_D)} \right) \quad (68)$$

is obtained. In the case that the radius is much greater than the Debye length, $a \gg \lambda_D$, the velocity varies from zero at the wall to the asymptotic

value $u_s = -\varepsilon\zeta E_z/\eta$ in a very thin layer of the order of λ_D . Furthermore, the bulk of the liquid in the capillary moves with velocity u_s , known as the electroosmotic slip velocity. For this case of $a \gg \lambda_D$, the slip velocity expression is valid in the general case where ζ is not restricted to be smaller than $k_B T/e$.

The average velocity and flow rate at zero pressure are

$$u_{\max} = u_s F(a^*) \quad Q_{\max} = \pi a^2 u_{\max}, \quad (69)$$

where $a^* = a/\lambda_D$ and

$$F(a^*) = \frac{2}{a^2} \int_0^a \left(1 - \frac{I_0(r/\lambda_D)}{I_0(a/\lambda_D)} \right) r \, dr = 1 - \frac{2I_1(a^*)}{a^* I_0(a^*)}. \quad (70)$$

The pressure difference between the capillary ends required to balance this flow rate is the maximum pressure that can be generated, and this is

$$\Delta p_{\max} = -\frac{8\varepsilon\zeta\Delta\Phi}{a^2} F(a^*). \quad (71)$$

Here $\Delta\Phi = E_z L$ is the potential difference applied between the ends of the capillary separated a distance L . In the thin double layer limit where $a \gg \lambda_D$, $F(a^*) \rightarrow 1$. Substitution yields $Q_{\max} = -\pi a^2 \varepsilon\zeta E_z/\eta$ and $\Delta p_{\max} = -8\varepsilon\zeta\Delta\Phi/a^2$. For capillary radii much smaller than the Debye length, $F(a^*) \rightarrow (a/\lambda_D)^2/8$.

To increase the pressure drop, the size of the micropipe can be reduced. This, however, reduces the flow rate. A way of increasing the pressure while not reducing much the flow rate is to use a bundle of parallel micropipes with small radius. In practice, EO pumps incorporate porous structures so that each pore acts as a tortuous capillary [48]. These porous structures can be visualized as a large number of tortuous micropipes in parallel. From this model, the theoretical maximum pressure is given by expression (71) and the maximum flow rate by [48]

$$Q_{\max} = -\frac{\psi}{\tau} \frac{\varepsilon\zeta A}{\eta} F(a^*), \quad (72)$$

where A is the cross-sectional area of the structure, ψ is its porosity (void volume divided by total volume of the porous medium), and τ is its

tortuosity defined as $(L_e/L)^2$ (L_e is the characteristic length of the tortuous path of the pores and L the length of the porous structure). From these expressions the number $\psi A/\tau\pi a^2$ can be seen as the effective number of EO capillaries with radius a connected in parallel which give the same flow rate as the porous structure.

3.1.2. Characteristics

3.1.2.1. Efficiency

Let us analyze the efficiency of a single capillary. The power consumption is given by the applied voltage multiplied by the electric current through the pump $P_{\text{in}} = IV$. The current transported by the liquid consists of two contributions [44]: that due to the bulk conductivity and that due to the surface conductivity including the convective current due to the electro-osmotic flow itself. Thus, one can write for a capillary

$$I = \pi a^2 \sigma E_z + 2\pi a \sigma_s E_z, \quad (73)$$

where σ_s is a specific surface conductivity. For a capillary we have

$$\frac{Q_{\text{max}}}{I} = \frac{\varepsilon \zeta}{\eta(\sigma + 2\sigma_s/a)} F(a^*). \quad (74)$$

Therefore, our estimation for the maximum efficiency is

$$\text{eff} = \frac{1}{4} \frac{\Delta p_{\text{max}} Q_{\text{max}}}{IV_{\text{app}}} = \frac{\Delta \Phi}{V_{\text{app}}} \frac{2(\varepsilon \zeta F(a^*))^2}{a^2 \eta(\sigma + 2\sigma_s/a)} \quad (75)$$

where V_{app} is the potential applied to the main circuit and, in general, is different from the potential difference at the ends of the capillary $\Delta \Phi$. In particular, the difference $V_{\text{app}} - \Delta \Phi$ should account for the threshold voltage needed to start the Faradaic reactions at the electrodes and the junction voltages at inlet and outlet of the capillary. The efficiency of a porous structure will be of the same order as that of a capillary since in the model, both Q and I are proportional to the number of capillaries in parallel and Δp and V are the same for all the capillaries.

In the case $\lambda_D \ll a$, the current will be given by the bulk contribution and, assuming an ideal situation where $V_{\text{app}} = \Delta \Phi$, the efficiency is

$$eff = \frac{2\varepsilon^2\zeta^2}{a^2\eta\sigma}. \quad (76)$$

We can see that, in this limit, the efficiency decreases with pore size a and with the product $\sigma\eta$, which is proportional to ionic concentration. It does not decrease with viscosity because the product $\sigma\eta$ is, in fact, almost independent of viscosity. In the general case, the efficiency is a maximum when a is of the order of λ_D [50, 48].

If the working liquid is relatively conductive, electroosmotic pumps can be very inefficient. Taking $\zeta = 0.1$ V, $a = 1\mu\text{m}$ and an aqueous solution of conductivity σ , we obtain $eff = 10^{-5}/\sigma$, with σ in SI units. The reason for this is that the two main origins for energy losses, Joule heating and viscous losses, both increase with conductivity. Joule heating is directly proportional to σ , given by $\int \sigma E^2 d\tau$. Viscous losses increase with σ because the shear stresses that balance the Coulomb force are confined to the thin diffuse layer, which is a decreasing function of σ . The viscous dissipation is greater in this case than when the viscous stresses are distributed across the entire capillary. The viscous dissipation is, for the thin diffuse layer, of the order of

$$P_v \sim \eta \frac{u_s^2 2\pi a L}{\lambda_D}. \quad (77)$$

This is of the order of a/λ_D times greater than for the case of viscous stresses evenly distributed in the capillary (as in the Poiseuille flow). However, the losses due to Joule heating are usually much greater, and Joule heating is the primary mechanism of power consumption at typical conditions of EO pumps [50]. The ratio between power consumption due to viscous stresses and due to Joule heating is of the order of

$$\frac{P_v}{P_j} \sim \frac{\eta u_s^2 2\pi a L / \lambda_D}{\sigma E^2 \pi a^2 L} = \frac{2\varepsilon^2 \zeta^2}{\eta \sigma \lambda_D a} = eff \frac{a}{\lambda_D} \quad (\lambda_D \ll a). \quad (78)$$

In this limit $\lambda_D \ll a$, we can see that $eff \sim (P_v/P_j)(\lambda_D/a)$, the product of two numbers smaller than one.

The EO micropump experiments presented in [51] show a maximum efficiency of around 0.004 for deionized water of conductivity $\sigma \sim 10^{-4} \text{ S m}^{-1}$, while the efficiency was around 0.022 for acetonitrile of

$\sigma \sim 10^{-6} \text{ S m}^{-1}$. The higher efficiency of acetonitrile is mainly due to its lower conductivity.

3.1.2.2. Liquids

Electrokinetic phenomena tend to disappear at high ionic concentrations. When the electrolyte conductivity is high, the Debye length becomes very small and comparable or smaller than the thickness of the Stern layer. Since the total double-layer voltage is shared between the compact and the diffuse layers, the reduction of the diffuse part leads to a reduction of the potential across it, i.e., a reduction of the zeta potential ζ . Applying a simple model of two capacitors in series (the compact-layer capacitor in series with the diffuse-layer capacitor) leads to the conclusion that ζ decreases with the squared-root of electrolyte concentration n^∞ . For values of $\sigma \sim 1 \text{ S m}^{-1}$, both capacitances are of the same order, (the Stern layer capacitance is of the order of $C_s \sim 0.3 \text{ F m}^2$ [44]). The prediction that $\zeta \propto 1/\sqrt{n^\infty}$ fails when the pH of the solution controls the surface charge [48]. However, ζ is still a decreasing function of ion concentration.

A lower bound for the conductivity of the liquid comes from a comparison between the electric field inside the double layer and the applied electric field. If the liquid conductivity is very small, the electric field inside the double layer (of the order of $\zeta/\lambda_D \sim k_B T/e\lambda_D$) becomes of the same order as the applied field required to have significant EO velocity. In this case, the distributions of ions in the capillary would be very distorted by the applied electric field. Therefore, it is not expected that electroosmosis can work properly at very low conductivity. For an applied field $E_z \sim 10^4 \text{ V m}^{-1}$, $\zeta \sim 0.025 \text{ V}$, the condition implies $\sigma > 10^{-7} \text{ S m}^{-1}$ for water (or $\sigma > 10^{-8} \text{ S m}^{-1}$ for nonpolar liquid with $\epsilon_r = 2$). Also, when the charge on the surface is governed by the process of deprotonation, as in the case of silica surfaces, the pH of the liquid is another parameter to be taken into consideration. The zeta potential is a strong function of pH, typically saturating at high and low pH [1]. According to Yao et al. [52], low buffer concentrations (below 0.1 mM) are impractical because pump operation generates prohibitively large fluctuations in pH.

Liquids that have been pumped using electroosmosis have conductivities that range from 10^{-6} to 1 S m^{-1} [50].

3.1.2.3. Problems

EO pumps operated continuously in DC mode suffer from inherent problems. Electrolysis generates gas bubbles, which must be prevented from coming into the pump channel. Redox reactions at the electrodes will eventually change the pH, which is a problem because the EO flow depends on it. For instance, under conditions of $Q = 0$ in order to obtain the maximum pressure, the liquid is recirculating in the pumping channels. The pH change introduced at the electrodes will stop the EO flow after a while when the buffer is depleted [53]. Traditionally, some of these problems are avoided by separating the electrodes from the EO pumping channels with an ion exchange system [45]. For example, in [54] the electrodes are placed in reservoirs separated by the channels by a porous glass disk. The disk allows for exchange of ions but not of bulk flow. The reservoirs are filled with buffers to reduce the changes in pH due to operation. Yao et al. [52] recombined the products of the reaction, where electrolytic gases were converted to water and reused by the system. Brask et al. [53] presented an EO pump that worked in AC mode in order to prevent the bubble formation and reduce the pH change problem. The pump was energized by square signal of ± 30 V and produced a pulsating flow. To rectify this oscillating flow, a system of valves was employed.

The high voltage usually required by EO pumps (traditionally in the kilovolt range) can be a drawback, especially for portable chips. A low voltage EO pump that produces high pressure (around 25 kPa at 10 V) has been realized by using a cascade pump design [55, 56]. The idea is to place several pumps in series in order to increase the pressure and each pump operates at low voltage (from 0 to 10 V) (see Fig. 6). Each pump consists of a narrow channel section, containing 10 parallel channels, followed by a wide single channel. The narrow channel section acts as a high pressure pump with forward electric field. In the wide channel section, the electric field is reversed, but here the channel is so wide that the generated back pressure is small compared to the previous pressure. Also, in order to reduce the voltage, the electrodes were in the flow path (gel salt bridge electrodes were used). Another way of reducing the voltage needed is to employ pumping based on transverse electrokinetic effects [57, 58]. It is based on the anisotropic response of a channel with obliquely oriented grooves to an applied field. The electric field is applied perpendicularly to the principal axis of the channel, resulting in flow in the axial direction. This allows for the generation of fluid velocities around $100\text{--}150\ \mu\text{m s}^{-1}$ for low applied voltages, around 10 V. Since the electrodes are inside the flow path, low ionic strength solutions are preferable to reduce generation of bubbles and to reduce local pH changes at the electrodes.

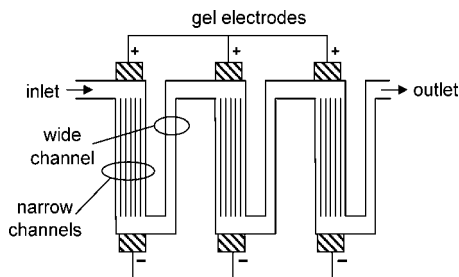


Fig. 6. Scheme of cascade pump by Takamura et al. [55]

The increment in temperature due to Joule heating can also be a problem. An order of magnitude estimate for the temperature increment is obtained by equating the generated heat in a capillary $\sigma E^2 \pi a^2 L$ to the heat flow through the lateral wall $\kappa(\partial T/\partial r)2\pi aL$. The estimation for the increment of temperature gives

$$\Delta T \sim a \frac{\partial T}{\partial r} \sim \frac{\sigma V^2 a^2}{2\kappa L^2}. \quad (79)$$

The smaller the radius of the cross-sectional area of the pump, the smaller the increment in temperature. As an example, the increment of temperature was around 20°C for $\sigma \sim 0.5 \text{ S m}^{-1}$ at an applied electric field of $6 \times 10^4 \text{ V m}^{-1}$ in the experiments of Tang et al. [59]. Therefore, the temperature rise can be excessive for conductivities equal or greater than 1 S m^{-1} .

3.1.2.4. Applications

Saline solutions with $\sigma \leq 1 \text{ S m}^{-1}$ can be pumped; therefore, possible applications range from bio-medical to chemical analysis, such as, the previously mentioned, on-chip liquid chromatography and on-chip electrophoresis separation. The energy efficiency can be very low for conductivities around 0.1 S m^{-1} , nevertheless there are many applications where this is not a limiting issue. Potential applications include the replacement of high-pressure pumps in micro-total-analysis-systems: for drug delivery, sample analysis, separation, and mixing processes. Another application is the use of closed-loop electroosmotic microchannels as cooling systems

for microelectronics [60]. Arrays of micropumps, temperature sensors, and fluid flow networks could be used to redistribute heat from hot spots that arise during microchip operation.

3.2. AC/IC Electroosmotic Pump

An alternating-current/induced-charge electroosmotic pump makes use of the Coulomb force on the induced-charge in the double layer [61, 62, 63]. Typically, the normal component of the electric field charges the double layer at the electrode/electrolyte interface, while the tangential electric field component produces a force on the induced charge in the diffuse layer that results in fluid motion [64, 65, 66]. Unidirectional fluid flow is typically obtained in two ways: arrays of asymmetric pairs of electrodes subjected to a single AC signal [6] or arrays of symmetric electrodes subjected to travelling-wave signals [67].

3.2.1. Pump Principle

Let us analyse the case of a travelling-wave potential that generates EO flow (see Fig. 7). We are going to apply the linear approximation of the double layer (Debye-Hückel approximation). Also, we assume that the applied potential is low enough so that Faradaic currents from the electrodes to the liquid are absent, i.e., we assume perfectly polarizable electrodes. At the level of the electrodes, $z = 0$, a travelling potential is applied that we model as $V(x, t) = V_0 \cos(kx - \omega t)$, where ω is the frequency of the applied signal and k is the wave-number that characterizes the spatial periodicity of the array. At the interface between electrodes and electrolyte, an electric double layer is formed. The frequency ω is low enough so that the double layer is in quasi-equilibrium. We assume that the Debye length is much smaller than any other length in the system and, in particular, $k\lambda_D \ll 1$. Above the array, the bulk electrolyte is electro-neutral characterized by its conductivity σ . The electric current follows Ohm's law $\mathbf{j} = \sigma \mathbf{E}$ and the electric potential holds Laplace's equation $\nabla^2 \Phi = 0$. The generated electric potential in the bulk is of the form (in phasor notation) $\Phi = \text{Re}[Ae^{-i(kx - \omega t) - kz}]$, where $i = \sqrt{-1}$. Here we have assumed that $kh \gg 1$, where h is the height of the upper wall of the device. The potential in the bulk at the limit of the Debye layer ($z = 0^+$) is related to the applied potential by the following boundary condition

$$\sigma \frac{\partial \Phi}{\partial z} = C_{DL} \frac{\partial(\Phi - V)}{\partial t} = i\omega C_{DL} (\Phi - V), \quad (80)$$

where C_{DL} is the double layer capacitance given by the series combination of the compact layer capacitance C_s and the Debye layer capacitance $C_{DL}^{-1} = C_s^{-1} + C_d^{-1}$. The previous boundary condition expresses the conservation of charge: the current arriving at the double layer charges the double-layer capacitor. From this equation, the constant A is obtained as $A = i\Omega V_0 / (1 + i\Omega)$, where $\Omega = \omega C_{DL} / \sigma k$. The Debye-Hückel theory gives the value of the diffuse double layer capacitance as $C_d = \varepsilon / \lambda_D$.

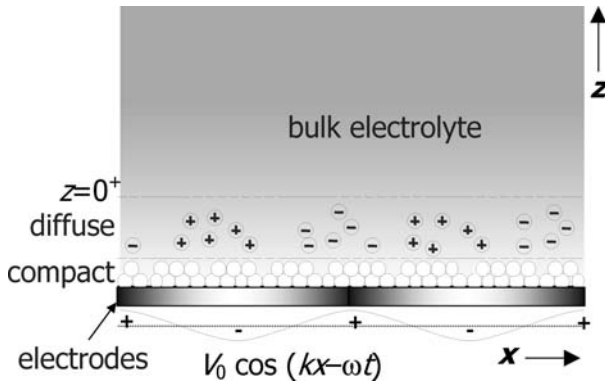


Fig. 7. Travelling wave electroosmotic pump. The dimension of the double layer is exaggerated.

The tangential electric field E_x produces a force on the induced charge in the diffuse layer $q_s = -C_d \zeta$. The potential drop across the diffuse layer ζ can be related to the total double-layer potential drop by $\zeta = C_s(V - \Phi) / (C_s + C_d)$. Although both electric field and induced charge are oscillating functions in time, the Coulomb force has a nonzero time-average that leads to a nonzero slip velocity. For electrical double layers in quasiequilibrium on perfectly polarizable electrodes, the classical calculation [68] gives for the electroosmotic slip velocity $u_s = -\varepsilon E_x \zeta / \eta$. The time-averaged slip velocity is given by [67, 69]

$$\langle u_s \rangle = \frac{1}{2} Re \left[\frac{-\varepsilon \zeta E_x^*}{\eta} \right] = \frac{C_s}{C_s + C_d} \frac{\varepsilon k V_0^2}{2\eta} \frac{\Omega}{1 + \Omega^2}, \quad (81)$$

where E_x^* is the complex conjugate of E_x . The EO slip velocity is a function of frequency with a maximum at $\Omega = 1$, and this maximum velocity is

$$\langle u_s \rangle_{\max} = \frac{C_s}{C_s + C_d} \frac{\varepsilon k V_0^2}{4\eta}. \quad (82)$$

Let us assume that there is also an array of electrodes subjected to the same travelling-wave in the upper wall. The fluid velocity from $z = 0$ to $z = h$ is constant under conditions of zero back pressure. The maximum average velocity is then equal to $u_{\max} = \langle u_s \rangle_{\max}$.

Now we can obtain the maximum flow rate and pressure generated by this pump. For a channel of rectangular cross section (height h and width w , $w \gg h$), and axial dimension L , the maximum flow rate and pressure are

$$Q_{\max} = \frac{C_s}{C_s + C_d} \frac{\varepsilon k V_0^2}{4\eta} wh \quad \Delta p_{\max} = \frac{C_s}{C_s + C_d} \frac{3\varepsilon k V_0^2 L}{h^2}. \quad (83)$$

According to these expressions, both pressure and flow rate increase if the wave-length of the periodic array is reduced (k is increased). The maximum pressure can be increased by reducing the height of the device, although at expenses of reducing the flow rate.

In experiments, the quadratic dependence on voltage is only observed at very low voltages. The velocity tends to a lower increment with voltage, which may be explained because of, at least, two mechanisms acting at the same time: (a) The potential ζ can not grow without limit because the charge in the diffuse double layer has an upper limit given by the size of the ions. Therefore, ζ saturates and the velocity becomes proportional to V . (b) If the potential is beyond the threshold voltage for the appearance of Faradaic currents, the double layer starts to leak charge. Experimentally and numerically, saturation of the velocity with voltage is observed [69, 70]. At still higher voltages, the flow changes direction, and generation of bubbles start to appear easily [71, 69, 72]. It seems that experimentally the AC EO mechanism provides a maximum slip velocity around $500 \mu\text{m s}^{-1}$.

3.2.2. Characteristics

3.2.2.1. Efficiency

In the theoretical model, no influence of the fluid velocity in the electric field is taken into account. In this limit, the mechanical power is negligible as compared to the power consumed by Joule heating. Therefore, our estimation for the total power consumption is $P_j \approx \int \sigma E_{\text{rms}}^2 d\tau$. The estimation for the efficiency is

$$\text{eff} = \frac{1}{4} \frac{Q_{\text{max}} \Delta p_{\text{max}}}{P_j} = \frac{3\varepsilon^2 V_0^2 k}{4(1 + C_d/C_s)^2 \sigma \eta h} \quad (84)$$

obtained at the optimum frequency that gives $\Omega = 1$. The expression for the efficiency is of the order of $\varepsilon u_{\text{max}}/\sigma h$, an electric Reynolds number, multiplied by the factor $C_s/(C_s + C_d)$. The efficiency increases for decreasing conductivity σ , decreasing height h , and increasing wave number k .

3.2.2.2. Liquids

The conductivity of the liquid to be pumped can not be very high. As the conductivity increases, the potential across the diffuse layer becomes much smaller than the applied potential across the total double layer. If we increase the total voltage in order to increase the potential ζ , Faradaic reactions can easily appear. Saline solutions in water that have been pumped using the AC/IC electroosmotic mechanism have conductivities below or equal to 0.1 S m^{-1} .

A lower bound for the conductivity of the liquid must also exist because the mechanism is based on the induced charge in the diffuse double layer. The mechanism can only work if there exists a clear distinction between a charged layer and an electro-neutral bulk liquid. Under the action of an electric field, the ion concentration should be greater than a certain value in order to have electro-neutrality in the bulk. Electro-neutrality does not apply if the parameter $\Lambda = \varepsilon E / e l n^\infty$ is of the order one or greater [12]. When $\Lambda \sim 1$, the electric field can create a charge layer of thickness $\sim l$ and charge density $\sim e n^\infty$. For a typical electric field of 10^5 V m^{-1} and a typical length of 10^{-5} m , the electric field destroys the electro-neutrality if the ion concentration is of the order

of $4 \times 10^{19} \text{ m}^{-3}$ ($\sigma \sim 3 \times 10^{-7} \text{ S m}^{-1}$) for a polar liquid like water and it is of the order of 10^{18} m^{-3} ($\sigma \sim 7 \times 10^{-9} \text{ S m}^{-1}$) for a nonpolar liquid of $\varepsilon \sim 2\varepsilon_0$.

Liquids that have been pumped using the AC/IC electroosmotic pump had conductivities in the range 10^{-4} to 0.1 S m^{-1} .

3.2.2.3. Problems

The applied voltage can not be very high in order to avoid Faradaic currents since the electrodes are in contact with the liquid. Therefore, low ionic strength solutions are preferable. The Faradaic reactions can degrade the electrodes after some time of operation. A way of reducing this problem is to use a dielectric coating on the electrodes, although this reduces the slip velocity for a given applied voltage. The use of titanium electrodes can be advantageous because titanium spontaneously form an oxide passivation layer that preserves them from degradation. As an advantage, because the pump is supposed to operate at voltages below the ionization potentials, the working liquid is not expected to suffer changes in its electrical properties.

3.2.2.4. Applications

Water saline solutions with $\sigma \leq 0.1 \text{ S m}^{-1}$ can be pumped, therefore, possible applications range from biomedical to chemical analysis. Typically, the generated pressure is small. However, these kinds of pumps have many potential applications for manipulating particles and fluids in closed microdevices, which do not require high pressure. For example, it may have applications in circular chromatography [73].

4. Magnetic Forces: DC and AC MHD Pumps

In a magnetohydrodynamic (MHD) pump, the force acting on the liquid is the Lorentz force. It appears when an electric current is subjected to a magnetic field. The magnetic force density is given by $\mathbf{f} = \mathbf{j} \times \mathbf{B}$. A simple way of looking at this expression is to consider that the magnetic force on a moving free charge, $\mathbf{F} = q\mathbf{v} \times \mathbf{B}$, is transmitted directly to the fluid, giving the previous body force density. We can distinguish two basic strategies of operation: a DC electric current is actuated by a static magnetic field (DC MHD micropump [7, 74, 75]) and an AC electric

current is actuated by an alternating magnetic field (AC MHD micropump [8, 76]).

4.1. DC MHD Micropump

The Lorentz force is generated by applying a static magnetic field, usually created by a permanent magnet, upon a DC electric current. The magnetic field generated by the current is usually negligible as compared to the applied magnetic field. In effect, from Ampere's law $\nabla \times \mathbf{B} = \mu \mathbf{j}$, where μ is the magnetic permeability, the magnetic field created by the current is of the order of $B_j \sim \mu_0 j l$ (l , typical distance and for nonmagnetic materials $\mu \approx \mu_0$, the permeability of vacuum). The ratio between the generated field B_j and the applied field B_0 is then $B_j/B_0 \sim \mu_0 j l/B_0$. An estimation for the current comes from the Lorentz force needed to generate a certain fluid velocity. From the Stokes equations, valid for low Reynolds number that are typical of microsystems, the comparison of the viscous term and the force density leads to a fluid velocity $u \sim j B l^2/\eta$. Therefore, the ratio is given by

$$\frac{B_j}{B_0} \sim \frac{\mu_0 \eta u}{B_0^2 l}, \quad (85)$$

which is usually very small. For example, taking $u \sim 10^{-3} \text{ m s}^{-1}$, $B_0 \sim 0.1 \text{ T}$, $l \sim 10^{-4} \text{ m}$, $\eta \sim 10^{-3} \text{ Pa s}$, the ratio is of the order of 10^{-6} . Therefore, the applied magnetic field is almost unperturbed by the electric current.

The electric current density for a moving conductor of conductivity σ is given by $\mathbf{j} = \sigma(\mathbf{E} + \mathbf{u} \times \mathbf{B})$. Except for liquid metals, the electric current driven by the electric field is much greater than that driven by the Lorentz term. In effect, the ratio is given by

$$\frac{|\mathbf{u} \times \mathbf{B}|}{E} \sim \frac{\sigma u B_0}{j} \sim \frac{\sigma B_0^2 l^2}{\eta}, \quad (86)$$

using the previous estimation for the liquid velocity $u \sim j B l^2/\eta$. The ratio is equal to the Hartmann number squared, $H = B l \sqrt{\sigma/\eta}$, and it is a measure of the ratio of the magnetic body force and the viscous force [74]. The value of H^2 is very small for liquids with conductivities

$\sigma \ll 10^6 \text{ S m}^{-1}$, such as electrolytic solutions. For instance, taking $B_0 \sim 1 \text{ T}$, $l \sim 10^{-4} \text{ m}$, $\eta \sim 10^{-3} \text{ Pa s}$ and $\sigma = 1 \text{ S m}^{-1}$ we obtain $H^2 \sim 10^{-5}$. Therefore, the electric current is given by the applied electric field for nonmetallic liquids in microsystems. For liquid metals, where the Hartmann number can be much greater than unity, the actual electric current distribution should be taken into account. The continuity of electric current $\nabla \cdot \mathbf{j} = 0$ must be considered and new induced electric fields appear. We restrict ourselves to the case of negligible Hartmann number.

4.1.1. Pumping Principle

Let us consider a straight conduit of length L with a rectangular cross section of height h and width w filled with an electrolyte, see Fig. 8. Perfectly conducting electrodes are placed on the two opposite sides of the conduit. The electrodes are subjected to a potential difference V , so there is an electric field $\mathbf{E} = E_0 \mathbf{e}_x$, with $E_0 = V/w$. There is also an applied homogeneous magnetic field in the vertical direction $\mathbf{B} = B_0 \mathbf{e}_y$. The liquid inside the conduit is subjected to the Lorentz force density $\mathbf{j} \times \mathbf{B}$ and fluid flow is generated. The conduit is considered very long so that fringe effects are neglected and the fluid flow is considered to have velocity only in the z -direction. The equation for the 1D velocity under a constant pressure gradient is

$$0 = \eta \nabla^2 u - \frac{\partial p}{\partial z} + \sigma E_0 B_0, \quad (87)$$

where we have considered the term $-\sigma u B_0^2$ to be negligible (Hartmann number much less than one). The flow has a profile similar to that of pressure-driven flow, and obeys Poiseuille law in microchannels [8, 75].

The pressure difference needed to stop the flow is

$$\Delta p_{\max} = \sigma E_0 B_0 L, \quad (88)$$

and the maximum average velocity and flow rate at zero pressure are approximately given by

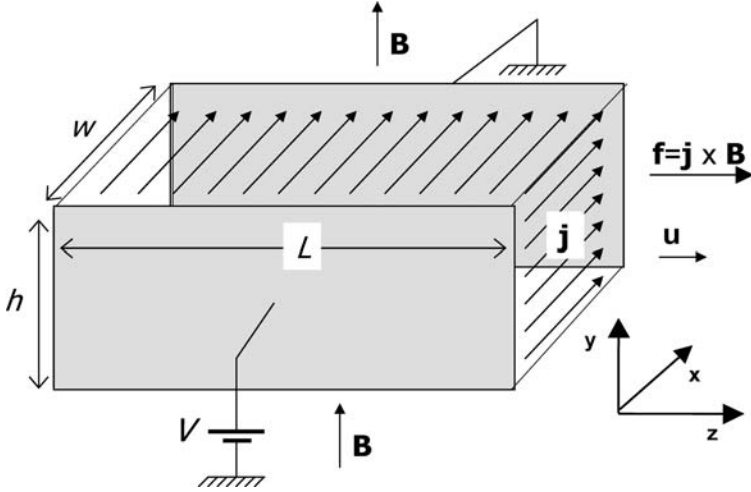


Fig. 8. Scheme of a magnetohydrodynamic pump

$$u_{\max} = \sigma E_0 B_0 \frac{D_h^2}{32\eta} \quad Q_{\max} = \frac{\sigma E_0 B_0 \pi D_h^4}{128\eta}, \quad (89)$$

where $D_h = 2wh/(w+h)$ is the hydraulic diameter of the conduit.

For liquid metals, the electric current density will surely be determined by the resistance of the total circuit and the applied voltage to it. It is usually the case that the applied voltage is much greater than uBw (the electromotive force generated by fluid motion). In this case, an estimation of the maximum pressure and maximum flow rate can be obtained from the previous expressions by substituting σE_0 for j , the mean current density in the channel.

4.1.2. Characteristics

4.1.2.1. Efficiency

Let us obtain an expression for the efficiency in the case when the Hartmann number is very small, such as the pumping of electrolytes. The power consumption is IV_{app} , where $I = \sigma E_0 hL$ is the current intensity through the conduit and V_{app} the potential applied to the circuit. The estimation for the maximum efficiency is

$$eff = \frac{1}{4} \frac{\Delta p_{\max} Q_{\max}}{IV_{\text{app}}} = \frac{V}{V_{\text{app}}} \frac{\sigma B_0^2 \pi D_h^4}{512 \eta h w} \sim \frac{V}{V_{\text{app}}} \frac{\sigma B_0^2 D_h^2}{128 \eta}, \quad (90)$$

where V is the potential difference between the channel walls. It can be seen that the efficiency is proportional to the Hartmann number squared. The efficiency of the pump is proportional to the conductivity and inversely proportional to the viscosity. It is inversely proportional to the square of the hydraulic diameter, which makes miniaturization more demanding. For $D_h = 100 \mu\text{m}$, $B = 1 \text{ T}$, $\sigma = 1 \text{ S m}^{-1}$, $\eta \sim 10^{-3} \text{ Pa s}$, $V/V_{\text{app}} \sim 1$, the maximum efficiency is $eff \sim 10^{-7}$. The estimated efficiency for the micropump experiments presented by Homsy et al. [75] is of the order of 10^{-9} for an applied voltage of 20 V and magnetic field of 0.4 T.

4.1.2.2. Liquids

The liquids that can be pumped by the MHD micropumps are typically conducting. For magnetic field intensities available using miniature permanent magnets (up to 1 T), the electric current needs to be of a certain value, which makes the required electric field to be inversely proportional to σ . A lower bound for the conductivity can be obtained assuming a limiting electric field around 10^7 V m^{-1} . With a required mean velocity of 10^{-3} m s^{-1} , hydraulic diameter $D_h \sim 10^{-3} \text{ m}$, applied magnetic field $B_0 \sim 1 \text{ T}$ and viscosity $\eta \sim 10^{-3} \text{ Pa s}$, we obtain a lower bound for the liquid conductivity of $\sigma \sim 3 \times 10^{-6} \text{ S m}^{-1}$ ($\sigma \sim 3 \times 10^{-4} \text{ S m}^{-1}$ for $D_h \sim 10^{-4} \text{ m}$). Another limitation working with liquids of low conductivity is the appearance of electroosmotic flow generated by the applied electric field that may affect adversely the MHD flow [75]. According to Homsy et al. electrolytes with ionic strengths from 0.01–0.1 M presented this problem, this is, electrolytes with conductivities around $0.1\text{--}1 \text{ S m}^{-1}$.

Mercury slugs, seawater, saline solutions and deionized water have been pumped using MHD micropumps [7, 74].

4.1.2.3. Problems

When aqueous solutions are actuated with DC voltage, bubble formation due to water electrolysis appears. Most of the MHD micropumps have integrated the electrodes directly into the pumping channel and, therefore, the formation of bubbles is problematic. To avoid that these bubbles get

into the channel, the electrodes were placed in reservoirs outside the channel in [75]. Frit-like structures connected the reservoirs to the channel in a similar way as is done in some electroosmotic pumps. The degradation of the electrodes due to Faradaic reactions is another issue [75]. The proper selection of electrode material and redox species can reduce this problem. Another way of reducing the problems due to Faradaic reactions is to use AC electric currents as in the AC MHD micropumps.

Joule heating can also be problematic. The generation of heat may increase the temperature in the channel up to values that are not appropriate. An estimate of the temperature rise can be done in a similar manner as was performed to obtain expression (79). The expression using the current density is

$$\Delta T \sim l \frac{\partial T}{\partial l} \sim \frac{j^2 l^2}{2\sigma\kappa}, \quad (91)$$

where l is a typical distance from the center of the channel to the lateral walls. It can be seen that, since a certain current density is required to generate a certain velocity, the increment of temperature is inversely proportional to σ . For a current density of 4000 A m^{-2} , $l \sim 5 \times 10^{-5} \text{ m}$, the temperature rise can be around 30 K for $\sigma \sim 10^{-3} \text{ S m}^{-1}$.

4.1.2.4. Applications

The performance of the pump increases with conductivity. Homsy et al. [75] showed that their MHD micropump was suitable for use with saline solutions of relatively high ionic strength, $\geq 0.1 \text{ M}$ (conductivity around $\sigma \geq 1 \text{ S m}^{-1}$). This is advantageous for the handling of physiological liquids that require higher buffer concentrations. MHD micropumps can also be used to produce secondary flows that may be beneficial for stirring, mixing [77] or to direct fluid into any desired path in a fluidic network [78]. Circular chromatographic applications may benefit from MHD micropumps [76].

Other applications for MHD micropumps include those where small quantities of liquid metals need to be pumped.

4.2. AC MHD Micropump

The AC MHD micropump uses both oscillating current and magnetic field to produce a continuous flow. The use of AC voltages reduces or avoids the electrolytic reactions needed to sustain the electric current and the associated formation of gas bubbles and electrode degradation [8]. As in

the DC MHD micropump, for electrolytic solutions the Hartmann number is small and the electric current is driven by the applied electric field, $\mathbf{j} = \sigma \mathbf{E}$. However, from Faraday's law there is an electric field generated by the oscillating magnetic field, $\nabla \times \mathbf{E}' = -\partial \mathbf{B} / \partial t$, that produces eddy currents in the channel. This electric field is negligible as compared to the electric field needed to drive significant current in electrolytes if

$$\frac{E'}{E_0} = \frac{\omega B l}{E_0} = \frac{\sigma \omega B l}{j_0} \ll 1, \quad (92)$$

where we have taken $E_0 = j_0 / \sigma$. For $\omega \leq 10^6 \text{ s}^{-1}$, $B \leq 1 \text{ T}$, $l = 10^{-4} \text{ m}$ and $\sigma \leq 1 \text{ S m}^{-1}$, we obtain $E' / E_0 \leq 0.05$ for a current density of $j_0 = 2000 \text{ A m}^2$, typical in experiments [76, 75]. Therefore, the electric field is given by the applied AC voltage. For liquid metals the situation is very different and the eddy currents dominate. We restrict again our analysis to the case of nonmetallic liquids.

4.2.1. Pump Principle

An electromagnet is placed under the channel and generates the oscillating magnetic field. The situation is equivalent to that of Fig. 8 with the applied voltage and magnetic field varying periodically in time with a single frequency ω .

To have continuous motion, the time-averaged Lorentz force $\langle \mathbf{f} \rangle = \int_0^T \mathbf{j} \times \mathbf{B} dt / T$ must be different from zero (here, $T = 2\pi / \omega$). The generated flow is actually pulsed; however, at high frequencies, only the time-averaged motion is observed.

The oscillating electric and magnetic fields are given by $\mathbf{E} = E_0 \cos \omega t \mathbf{e}_x$ and $\mathbf{B} = B_0 \cos(\omega t + \phi) \mathbf{e}_y$, respectively. The equation for the time-averaged velocity is still given by (87), but the driving time-averaged force density is now $(1/2)\sigma E_0 B_0 \cos \phi$. The control of the phase allows for controlling both the speed and flow direction [8]. The expressions for the maximum pressure, maximum velocity and maximum flow rate are equivalent to the DC case, changing $E_0 B_0$ by $E_0 B_0 \cos \phi / 2$.

In experiments, the AC magnetic field amplitude is not constant but it is a function of the frequency of the electromagnet circuit [8, 76], typically decreasing for frequencies greater than several kHz. It is desirable that the

frequency is high so that electrolysis and bubble formation is avoided. Electric currents can be higher at higher frequencies without bubble formation. Therefore, there is an optimum frequency of operation in order to maximize $|\mathbf{j} \times \mathbf{B}|$.

4.2.2. Characteristics

4.2.2.1. Efficiency

The efficiency is less than in the case of DC MHD pump for similar electric and magnetic field amplitudes because the power consumption includes, in addition to the power consumed by the electric current in the channel, the power needed to feed the electromagnet. The estimate for the maximum efficiency is, therefore,

$$eff \sim \frac{V}{V_{app}} \frac{\sigma B_{rms}^2 D_h^2}{128\eta(1+\alpha)}, \quad (93)$$

where α is the ratio between the power consumed by the electromagnet and the power consumed by the electric current in the channel.

4.2.2.2. Liquids

As for the DC MHD pump, liquids that can be pumped are typically conducting. The lower bounds for the conductivity previously obtained for the DC MHD pump are also valid here. The actuation of liquid metals can be problematic for the AC MHD pump because the generated eddy currents in the liquid metal are not negligible and might have negative effects. They can heat the sample and the fluid flow might be quite different from what is expected. The liquids that were pumped by the AC MHD micropump of Lemoff and Lee [8] have conductivities from around 0.1 to around 10 S m⁻¹.

4.2.2.3. Problems

The generation of heat in the channel due to Joule heating is also present here as for the DC MHD pump. However, new sources of heat appear such as induction heating in the magnetic core material of the electromagnet and heating by eddy currents in the electrodes of the channel [76]. These effects limit the intensity of the AC magnetic field that can be obtained at high frequencies and, as a result, the fluid flow. The problem of the eddy currents in the electrodes can be reduced by laminating the electrodes, in a similar ways as is done in transformers [76].

4.2.2.4. Applications

The applications are similar to those of the DC MHD pump. The pumping of small samples of liquid metals by using AC MHD micropumps might be problematic.

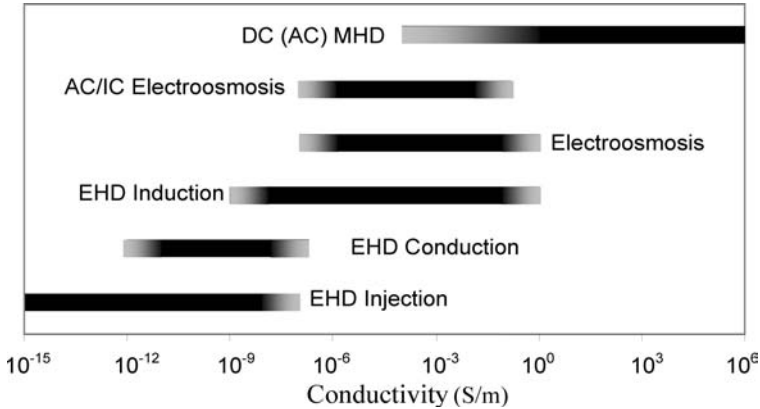


Fig. 9. Estimated conductivity ranges of the working fluid for operation of the different micropumps

5. Comparisons and Conclusions

In a first approach, each micropump can actuate liquids within a certain range of conductivities. The choice of a micropump should take into account this fact. For instance, very insulating liquids can be actuated by the EHD injection micropump, while liquid metals can be actuated by the DC MHD micropump. Figure 9 shows estimated conductivity ranges of the working fluid that each micropump can actuate. These ranges have been obtained using either values from theory or from experiments for microsystems. The limits of these ranges are necessarily fuzzy, since they depend on several parameters and geometry.

With respect to the performance of the different pumps, Table 1 summarizes theoretical expressions for the estimated maximum pressure and maximum flow rate for each micropump, and Table 2 shows experimental values of some selected works. For the theoretical expressions, we consider a given channel where the electric or magnetic forces are acting on the working fluid. The channel has the following dimensions: axial length equal to L , and cross-section of width w and height h . We have

used in some expressions the hydraulic diameter $D_h = 2wh/(w+h)$. The injection pump presents two limits: (a) electro-migration is negligible in front of convection, $\mu E \ll u$, and (b) convection is negligible in front of electro-migration $u \ll \mu E$. The second case ($u \ll \mu E$) leads to values for the maximum pressure and flow rate that are 9/16 smaller than the first case ($\mu E \ll u$). For the induction pump, we have neglected $\beta = (1/\varepsilon)\partial\varepsilon/\partial T$ in front of $\alpha = (1/\sigma)\partial\sigma/\partial T$ because it is usually much smaller. For the electroosmotic pump, we have written the expressions for the case $\lambda_D \ll D_h$. In the case of AC/IC EO pump we have written the expression corresponding to $w \gg h$ as an approximation. For the AC magnetohydrodynamic micropump, the root-mean-square values of the AC magnetic field B_{rms} and voltage V_{rms} should be employed.

Table 1. Estimated maximum pressure and flow rate generated for the different mechanisms in a channel of length L , width w , and height h .

Mechanism	Δp_{max}	Q_{max}
EHD injection	$\Lambda 2\varepsilon V^2/L^2$	$\Lambda \pi D_h^4 \varepsilon V^2/64\eta L^3$
EHD induction	$0.85\varepsilon V^2/L^2$	$0.85\pi D_h^4 \varepsilon V^2/128\eta L^3$
EHD induction	$\varepsilon V^2 \alpha\Delta T /L^2$	$\pi D_h^4 \varepsilon V^2 \alpha\Delta T /128\eta L^3$
AC/IC electroosmosis	$32\varepsilon \zeta V/D_h^2$	$wh\varepsilon \zeta V/\eta L$
AC/IC electroosmosis	$6\varepsilon k V_{\text{rms}}^2 L/h^2 (1 + C_d/C_s)$	$\varepsilon k V_{\text{rms}}^2 wh/2\eta (1 + C_d/C_s)$
(DC or AC) MHD	$\sigma VBL/w$	$\pi D_h^4 \sigma VB/128\eta w$

For the injection case, $\Lambda = 1$ if $\mu E \ll u$, and $\Lambda = 9/16$ if $u \ll \mu E$.

With respect to the experimental values of Table 2, some Δp_{max} values have been obtained by multiplying the flow rates by estimations of the hydraulic resistance of the system. The systems would be able to provide

maximum pressures of the order of the estimated ones. We have also included the length L and cross-sectional area S of the estimated liquid volumes actuated by the micropumps because the hydraulic power delivered by a micropump is usually an increasing function of volume. In fact, connecting micropumps in series increases the maximum pressure and connecting micropumps in parallel increases the maximum flow rate.

Table 2. Selected experimental values of micropumps.

Reference	Type	Working liquid	Δp_{\max} (Pa)	Q_{\max} (mm ³ s ⁻¹)	V (V)	S (mm ²)	L (mm)
Darabi and Wang [27]	Injection	HFE-7100	500	75	180	0.5	20
Richter Sandmaier [2]	Injection	Ethanol	2,500	200	700	9	0.35
Ahn Kim[24]	Injection	Ethyl alcohol	175	0.25	100	0.3	15
Feng Seyed-Yagoobi [31]	Conduction	R-123	270	4,000	10 ⁴	80	90
Fuhr et al. [38] ^a	Induction	Water	6	7.5×10^{-3}	14	0.025	4
Felten et al. [39] ^a	Induction	Water	2.7	3×10^{-4}	3.5	0.003	0.24
Yao et al. [52]	Electroos.	Borate buffer	1.3×10^5	550	100	1300	1
Chen Santiago [50]	Electroos.	Water	3.3×10^4	0.25	1,000	0.034	1
Takamura et al. [55]	Electroos.	Phosphate buffer	800	7×10^{-3}	10	0.003	1.2
Wang et al. [51]	Electroos.	Water	3×10^5	0.05	6,000	0.008	60
Studer et al. [71] ^a	AC/IC EO	Water	90	1.4×10^{-3}	3.5	0.002	6
García et al. [72] ^a	AC/IC EO	Water	0.14	0.04	2.1	0.2	2
Homsy et al. [75] ^a	DC MHD	1 M KCl solution	28	8.3×10^{-3}	20	0.01	16
Eijkel et al. [76] ^a	AC MHD	1 M KCl solution	26	1.2×10^{-4}	2.8	0.006	60

^a The value Δp_{\max} is estimated from flow rate and hydraulic resistance.

To have a rough idea of the pressure difference needed to obtain a given flow rate in a microfluidic system, let us consider that our external load is a microchannel of cross section $100\mu\text{m} \times 100\mu\text{m}$ and length L . The channel is folded and compacted in a small area (of the order of 1 cm^2) so that the length L can be something between 1 mm and 1 m. We would like to obtain a liquid velocity around 1 mm s^{-1} , that can be sufficient for a microsystem ($Q = 10^{-11}\text{ m}^3\text{ s}^{-1} = 0.01\text{ mm}^3\text{ s}^{-1}$ in this example). From (13), the pressure required if the liquid is water is of the

order of $\Delta p \sim 4000L$ Pa (L in meters). Therefore, we have a range of pressures from 4 to 4000 Pa that are required to be generated by the micropumps.

We can see in Table 2 that the EO pumps can provide these pressures and flow rates. We remember here that a single capillary of small radius ($\sim 1\mu\text{m}$) can generate high pressure, although the generated flow rate will be small. The EO pumps that generate high pressure and flow rate are typically made of porous structures [1]. These pumps can be visualized as a bundle of tortuous capillaries in parallel.

The injection pump of Richter and Sandmaier [2] could also work in all the pressure range of our example provided that some micropumps are placed in series in order to increase the pressure. According to the theoretical expressions, the maximum pressure that the EHD injection micropump can generate is of the order of εE^2 , for only one stage. Electric breakdown will limit the maximum attainable pressure, and this is a factor to be taken into account. The breakdown field can vary from 10 to 100 MV m^{-1} depending on liquid, impurities, and geometry. For the experiments of Darabi and Wang [27], a breakdown electric field of 11 MV m^{-1} was observed for HFE-7100 liquid. Taking a breakdown electric field of around 10 MV m^{-1} , a maximum attainable pressure of $\Delta p_{\text{max}} = \varepsilon_r 900 \text{ Pa}$ is obtained (ε_r , relative permittivity). Of course, the maximum attainable pressure generated by one stage can be much higher if the breakdown field is higher: it may be very high for very pure dielectric liquids ($> 100 \text{ MV m}^{-1}$).

For the conduction pump, the upper bound for the generated pressure is governed by the maximum electric field before ion injection reverses the flow direction [3]. The pressure generated (around 300 Pa at 10 kV) by the conduction pump of Feng and Seyed-Yagoobi [31] may be enough for some microfluidic applications. Although the dimensions of this pump are in the millimeter to centimeter scale, it seems possible to build a real micropump based on this mechanism.

In the case of the induction micropump, the theoretical value for the generated pressure is much smaller than εE^2 because of the factor $\alpha \Delta T$, that can be very small. The maximum electric field is also limited by EHD instabilities [36, 38]. From the theoretical expressions for the travelling-wave device, these induction micropumps may provide higher pressures if the height of the device is of the order of the gap and electrode width. This procedure, of course, reduces the flow rate.

The AC/IC EO micropump generates very little pressure (see Table 2). However, looking at the theoretical expressions, reducing the height h of

the actuated microchannel would increase the generated pressure (proportional to $1/h^2$). This procedure reduces the flow rate and, in order to maintain it, the strategy should be to use as many micropumps connected in parallel as possible. However, this may not be easy or possible to realize experimentally.

The MHD micropumps also provide little pressure. The electric current, σE , can be increased but it is limited by Joule heating effects. It is also very difficult to increase the magnetic field beyond 1 T.

Looking at Table 2, we can see that, at present, only the electroosmotic and EHD injection micropumps perform well in terms of generating enough pressure and flow rate for a microfluidic system like the one described in the example. However, there are many possible applications where strong pumping is not required and where the microfluidic system can be actuated by electric or magnetic forces distributed in all, or a significant part, of the device: cooling of special elements [28], circular chromatographic applications [76,73], pumping and local control of flow in microfluidic networks [57,78], or pumping of secondary flows that can enhance stirring and mixing [43,77].

The voltage required to operate a micropump is also an important factor to be considered, especially for portable microsystems where batteries would be used. The voltage used is included in table 2. The use of pumps connected in series like the cascade pump of Takamura et al. [55] reduces the required voltage. The use of electrodes inside the microchannel together with techniques like transverse electrokinetic effects [57], or AC/IC electroosmosis [6], also requires a low voltage.

To conclude, the choice of a particular integrated micropump should consider, among other factors, the properties of the working fluid (in particular the conductivity), the voltage required to operate the micropump, the generation of gases by the electrochemical reactions and the generation of heat by the Joule effect.

Acknowledgments

The author is grateful to Prof. Antonio Castellanos and Dr. Alberto T. Pérez for their critical readings of the manuscript and their valuable comments. This work was supported by the Spanish government agency DGCyT under contract FIS2006-0364 and the regional government Junta de Andalucía under project FQM-421.

References

1. Laser D.J. and Santiago J.G., A review of micropumps, *J. Micromech. Microeng.*, **14**, R35–R64 (2004)
2. Richter A. and Sandmaier H., An electrohydrodynamic micropump. In: *Proceedings of Micro Electro Mechanical Systems, 1990*. ‘An Investigation of

- Micro Structures, Sensors, Actuators, Machines and Robots', IEEE, pp. 99–104 (1990)
3. Atten P. and Seyed-Yagoobi J., Electrohydrodynamically induced dielectric liquid flow through pure conduction in point/plane geometry, *IEEE Trans. Dielectr. Electr. Insul.*, **10**, 27–36 (2003)
 4. Fuhr G., Hagedorn R., Müller T., Benecke W. and Wagner B., Microfabricated electrohydrodynamic (EHD) pumps for liquids of higher conductivity, *J. Microelectromech. Syst.*, **1**, 141–146 (1992)
 5. Pretorius V., Hopkins B.J. and Schieke J.D., Electro-osmosis: A new concept for high-speed liquid chromatography, *J. Chrom.*, **99**, 23–30 (1974)
 6. Brown A.B.D., Smith C.G. and Rennie A.R., Pumping of water with AC electric fields applied to asymmetric pairs of microelectrodes, *Phys. Rev. E*, **63**, 016305 (2000)
 7. Jang J. and Lee S.S., Theoretical and experimental study of MHD (magnetohydrodynamic) micropump, *Sensors Actuators*, **80**, 84–89 (2000).
 8. Lemoff A.V. and Lee A.P., An AC magnetohydrodynamic micropump, *Sensors Actuators B*, **63**, 178–185 (2000)
 9. Schmidt W.F., Conduction mechanisms in liquids. In: Bartnikas R. (ed) *Electrical Insulating Liquids. Engineering Dielectrics, Vol III*. American Society for Testing and Materials, Philadelphia, PA, (1994)
 10. Castellanos A., Basic concepts and equations in Electrohydrodynamics. Part I. In: Castellanos A. (ed) *Electrohydrodynamics*. Springer-Verlag, New York, (1998)
 11. Castellanos A., Ramos A., González A., Green N.G. and Morgan H., Electrohydrodynamics and dielectrophoresis in microsystems: Scaling laws. *J. Phys. D: Appl. Phys.*, **36**, 2584–2597 (2003)
 12. Saville D.A., Electrohydrodynamics: The Taylor-Melcher leaky dielectric model. *Annu. Rev. Fluid Mech.*, **29**, 27–64 (1997)
 13. Zhakin A.I., Conduction phenomena in dielectric liquids. Part II. In: Castellanos A. (ed) *Electrohydrodynamics*. Springer-Verlag, New York (1998)
 14. Bard A.J. and Faulkner L.R., *Electrochemical Methods: Fundamentals and Applications, 2nd Edition*. John Wiley and Sons, New York (2001)
 15. Haus H.A. and Melcher J.R., *Electromagnetic Fields and Energy*, Prentice Hall, Englewood Cliffs, NJ (1989)
 16. Stone H.A., Stroock A.D. and Ajdari A., Engineering flows in small devices: Microfluidics toward a Lab-on-a-Chip, *Annu. Rev. Fluid Mech.*, **36**, 381–411 (2004)
 17. Stratton J.A., *Electromagnetic Theory*, McGraw Hill, New York (1941)
 18. Jones T.B., Liquid dielectrophoresis on the microscale, *J. Electrostatics*, **51–52**, 290–299 (2001)
 19. Stuetzer O.M., Instability of certain electrohydrodynamic systems, *Phys. Fluids.*, **2**, 642–648 (1959)
 20. Stuetzer O.M., Ion drag pumps, *J. Appl. Phys.*, **31**, 136–146 (1960)
 21. Pickard W.F., Ion drag pumping. I. Theory, *J. Appl. Phys.*, **34**, 246–250 (1963)

22. Pickard W.F., Ion drag pumping. II. Experiment, *J. Appl. Phys.*, **34**, 251–258 (1963)
23. Richter A., Plettner A., Hofmann K.A. and Sandmaier H., Electrohydrodynamic pumping and flow measurement. In: *Proceedings of Micro Electro Mechanical Systems*, MEMS '91. 'An Investigation of Micro Structures, Sensors, Actuators, Machines and Robots', IEEE, pp. 271–276 (1991)
24. Ahn S.H. and Kim Y.K., Fabrication and experiment of planar micro ion drag pump, *International Conference on Solid State Sensors and Actuators*, 1997. Transducers'97, **1**, 373–376 (1997)
25. Darabi J., Rada M., Ohadi M. and Lawler J., Design, fabrication, and testing of an electrohydrodynamic ion-drag micropump, *J. Microelectromech. Syst.*, **11**, 684–690 (2002)
26. Crowley J.M., Wright G.S. and Chato J.C., Selecting a working fluid to increase the efficiency and flow rate of an EHD pump, *IEEE Trans. Ind. Appl.*, **26**, 42–49 (1990)
27. Darabi J. and Wang H., Development of an electrohydrodynamic injection micropump and its potential application in pumping fluids in cryogenic cooling systems, *J. Microelectromech. Syst.*, **14**, 747–755 (2005)
28. Foroughi P., Benetis V., Ohadi M., Zhao Y. and Lawler J., Design, testing and optimization of a micropump for cryogenic spot cooling applications. In: *Proceedings of Semiconductor Thermal Measurement and Management Symposium* Twenty First Annual IEEE Conference, pp. 335–340 (2005)
29. Seyed-Yagoobi J., Electrohydrodynamic pumping of dielectric liquids, *J. Electrostatics*, **63**, 861–869 (2005)
30. Jeong S. and Seyed-Yagoobi J., Experimental study of electrohydrodynamic pumping through conduction phenomenon, *J. Electrostatics*, **56**, 123–133 (2002)
31. Feng Y. and Seyed-Yagoobi J., Understanding of electrohydrodynamic conduction pumping phenomenon, *Phys. Fluid.*, **16**, 2432–2441 (2004)
32. Thomson J.J. and Thomson G.P., *Conduction of Electricity Through Gases*, 3rd edition, Cambridge University Press, Cambridge (1928)
33. Langevin P., Recombinaison et mobilités des ions dans les gaz. *Annales de Chimie et de Physique*, **28**, 433 (1903)
34. Pontiga F., Sobre la estabilidad de una capa de líquido sometida a un campo eléctrico y un gradiente térmico, PhD Thesis, University of Seville (1992)
35. Melcher J.R. and Taylor G.I., Electrohydrodynamics: A review of the role of interfacial shear stresses *Ann. Rev. Fluid Mech.*, **1**, 111–146, (1969)
36. Melcher J.R. and Firebaugh M.S., Travelling-wave bulk electroconvection induced across a temperature gradient, *Phys. Fluids.*, **10**, 1178–1185, (1967)
37. Müller T., Arnold W.M., Schnelle T., Hagedorn R., Fuhr G. and Zimmermann U., A traveling-wave micropump for aqueous solutions: Comparison of 1 g and μ g results. *Electrophoresis*, **14**, 764–772 (1993)
38. Fuhr G., Schnelle T. and Wagner B., Travelling wave-driven microfabricated electrohydrodynamic pumps for liquids, *J. Microelectromech. Syst.*, **4**, 217–226 (1994)

39. Felten M., Geggier P., Jäger M. and Duschl C., Controlling electrohydrodynamic pumping in microchannels through defined temperature fields, *Phys. Fluids*, **18**, 051707 (2006)
40. Green N.G., Ramos A., González A., Castellanos A. and Morgan H., Electric field induced fluid flow on microelectrodes: The effect of illumination. *J. Phys. D: Appl. Phys.*, **33**, L13–L17 (2000)
41. González A., Ramos A., Castellanos A., Green N.G. and Morgan H., Electrothermal flows generated by alternating and rotating electric fields in microsystems, *J. Fluid Mech.*, **564**, 415–433 (2006)
42. Ramos A., Morgan H., Green N.G. and Castellanos A., AC electrokinetics: A review of forces in microelectrode structures, *J. Phys. D: Appl. Phys.*, **31**, 2338–2353 (1998)
43. Sigurdson M., Wang D. and Meinhart C.D., Electrothermal stirring for heterogeneous immunoassays, *Lab Chip*, **5**, 1366–1373 (2005).
44. Hunter R.J., *Zeta Potential in Colloid Science*. Academic Press, San Diego (1981).
45. Dasgupta P.K. and Liu S., Electroosmosis: A reliable fluid propulsion system for flow injection analysis, *Anal. Chem.*, **66**, 1792–1798 (1994)
46. Manz A., Effenhauser C.S., Burggraf N., Harrison D.J., Seiler K. and Fluri K., Electroosmotic pumping and electrophoretic separations for miniaturized chemical analysis systems, *J. Micromech. Microeng.*, **4**, 257–265 (1994)
47. Jacobson S.C., Hergenroder R., Koutny L.B. and Ramsey J.M., Open-channel electrochromatography on a microchip, *Anal. Chem.*, **66**, 2369–2373 (1994)
48. Yao S. and Santiago J.G., Porous glass electroosmotic pumps: Theory, *J. Colloid Interface Sci.*, **268**, 133–142 (2003)
49. Rice C.L. and Whitehead R., Electrokinetic flow in a narrow cylindrical capillary, *J. Phys. Chem.*, **69**, 4017–4024 (1965)
50. Chen C.H. and Santiago J.G., A planar electroosmotic micropump, *J. Microelectromech. Syst.*, **11**, 672–683 (2002)
51. Wang P., Chen Z. and Chang H.H., A new electro-osmotic pump based on silica monoliths, *Sensors Actuators B*, **113**, 500–509 (2006)
52. Yao S., Hertzog D.E., Zeng S., Mikkelsen J.C. and Santiago J.G., Porous glass electroosmotic pumps: Design and experiments, *J. Colloid Interface Sci.*, **268**, 143–153 (2003)
53. Brask A., Snakenborg D., Kutter J.P. and Bruus H., AC electroosmotic pump with bubble-free palladium electrodes and rectifying polymer membrane valves, *Lab Chip*, **6**, 280–288 (2006)
54. Lazar I.M. and Karger B.L., Multiple open-channel electroosmotic pumping system for microfluidic sample handling, *Anal. Chem.*, **74**, 6259–6268 (2002)
55. Takamura Y., Onoda H., Inokuchi H., Adachi S., Oki A. and Horiike A., Low-voltage electroosmosis pump for stand-alone microfluidics devices, *Electrophoresis*, **24**, 185–192 (2003)
56. Brask A., Goranovic G. and Bruus H., Theoretical analysis of the low-voltage cascade electro-osmotic pump, *Sensors Actuators B*, **92**, 127–132 (2003)

57. Gitlin I., Stroock A.D., George M., Whitesides G.M. and Ajdari A., Pumping based on transverse electrokinetic effects, *Appl. Phys. Lett.*, **83**, 1486–1488 (2003)
58. Ajdari A., Transverse electrokinetic and microfluidic effects in micro-patterned channels: Lubrication analysis for slab geometries, *Phys. Rev. E*, **65**, 016301 (2002)
59. Tang G., Yan D., Yang C., Gong H., Chai J.C. and Lam Y.C., Assessment of Joule heating and its effects on electroosmotic flow and electrophoretic transport of solutes in microfluidic channels, *Electrophoresis*, **27**, 628–639 (2006)
60. Jiang L., Mikkelsen J., Koo J.-M., Huber D., Yao S., Zhang L., Zhou P., Maveety J.G., Prasher R., Santiago J.G., Kenny T.W. and Goodson K.E., Closed-loop electroosmotic microchannel cooling system for VLSI circuits, *IEEE Trans. Compon. Packag. Technol.*, **25**, 347–355 (2002)
61. Ramos A., Morgan H., Green N.G. and Castellanos A., AC electric-field-induced fluid flow in microelectrodes, *J. Colloid Interface Sci.*, **217**, 420–422 (1999)
62. Ajdari A., Pumping liquids using asymmetric electrode arrays, *Phys. Rev. E*, **61**, R45–R48 (2000)
63. Bazant M.Z. and Squires T.M., Induced-charge electrokinetic phenomena: Theory and microfluidic applications, *Phys. Rev. Lett.*, **92**, 066101 (2004)
64. Green N.G., Ramos A., González A., Morgan H. and Castellanos A., Fluid flow induced by non-uniform AC electric fields in electrolytes on microelectrodes I: Experimental measurements. *Phys. Rev. E*, **61**, 4011–4018, (2000)
65. González A., Ramos A., Green N.G., Castellanos A. and Morgan H., Fluid flow induced by non-uniform AC electric fields in electrolytes on micro-electrodes II: A linear double-layer analysis. *Phys. Rev. E*, **61**, 4019–4028, (2000)
66. Green N.G., Ramos A., González A., Morgan H. and Castellanos A., Fluid flow induced by non-uniform AC electric fields in electrolytes on microelectrodes III: Observation of streamlines and numerical simulations. *Phys. Rev. E*, **66**, 026305, (2002)
67. Cahill B.P., Heyderman L.J., Gobrecht J. and Stemmer A., Electro-osmotic streaming on application of traveling-wave electric fields, *Phys. Rev. E*, **70**, 036305 (2004)
68. Levich V.G., *Physicochemical Hydrodynamics*. Prentice-Hall, Englewood Cliffs, NJ (1962)
69. Ramos A., Morgan H., Green N.G., González A. and Castellanos A., Pumping of liquids with traveling-wave electroosmosis, *J. Appl. Phys.*, **97**, 084906 (2005)
70. Olesen L.H., Bruus H. and Ajdari A., AC electrokinetic micropumps: The effect of geometrical confinement, Faradaic current injection, and nonlinear surface capacitance, *Phys. Rev. E*, **73**, 056313 (2006)

71. Studer V., Pepin A., Chen Y. and Ajdari A. An integrated AC electrokinetic pump in a microfluidic loop for fast and tunable flow control. *Analyst*, **129**, 944–949 (2004)
72. García-Sánchez P., Ramos A., Green N.G. and Morgan H., Experiments on AC electrokinetic pumping of liquids using arrays of microelectrodes, *IEEE Trans. Dielectr. Electr. Insul.*, **13**, 670–677 (2006)
73. Debesset S., Hayden C.J., Dalton C., Eijkel J.C.T. and Manz A., An AC electroosmotic micropump for circular chromatographic applications, *Lab Chip* **4**, 396–400 (2004)
74. Zhong J., Yi M. and Bau H.H., Magneto hydrodynamic (MHD) pump fabricated with ceramic tapes, *Sensors Actuators*, **96**, 59–66 (2002)
75. Homsy A., Koster S., Eijkel J.C., van den Berg A., Lucklum F., Verpoorte E. and de Rooij N.F., A high current density DC magnetohydrodynamic (MHD) micropump, *Lab Chip*, **5**, 466–471 (2005)
76. Eijkel J.C.T., Dalton C., Hayden C.J., Burt J.P.H. and Manz A., A circular AC magnetohydrodynamic micropump for chromatographic applications, *Sensors Actuators B*, **92**, 215–221 (2003)
77. Bau H.H., Zhong J. and Yi M., A Minute magneto hydro dynamic (MHD) mixer, *Sensors Actuators B*, **79**, 205–213 (2001)
78. Bau H.H., Zhu J., Qian S. and Xiang Y., A Magneto-hydrodynamically controlled fluidic network, *Sensors Actuators B*, **88**, 205–216 (2003)

Microfluidic Technologies for Miniaturized Analysis
Systems

Hardt, S.; Schönfeld, F. (Eds.)

2007, XXI, 616 p., Hardcover

ISBN: 978-0-387-28597-9